

Supplementary Material for “Noise-Tolerant Optomechanical Entanglement via Synthetic Magnetism”

Deng-Gao Lai,^{1,2} Jie-Qiao Liao,^{1,*} Adam Miranowicz,^{2,3} and Franco Nori^{2,4,5}

¹Key Laboratory of Low-Dimensional Quantum Structures and Quantum Control of Ministry of Education, Key Laboratory for Matter Microstructure and Function of Hunan Province, Department of Physics and Synergetic Innovation Center for Quantum Effects and Applications, Hunan Normal University, Changsha 410081, China

²Theoretical Quantum Physics Laboratory, RIKEN Cluster for Pioneering Research, Wako-shi, Saitama 351-0198, Japan

³Institute of Spintronics and Quantum Information, Faculty of Physics, Adam Mickiewicz University, 61-614 Poznań, Poland

⁴RIKEN Center for Quantum Computing (RQC), Wako-shi, Saitama 351-0198, Japan

⁵Physics Department, The University of Michigan, Ann Arbor, Michigan 48109-1040, USA

In this Supplementary Material, we present the detailed results on the noise-tolerant quantum entanglement in optomechanical networks. Specifically, this document consists of five sections: (i) the Langevin equations, the dark mode, and its breaking in a three-mode optomechanical system; (ii) optomechanical entanglement enabled by the dark-mode breaking, which is induced by synthetic magnetism; (iii) Dark modes and their breaking in optomechanical networks; (iv) dark-mode-immune entanglement networks; and (v) possible experimental realizations of the system.

I. THE LANGEVIN EQUATIONS, THE DARK MODE, AND ITS BREAKING

In this section, we derive the quantum Langevin equations of a two-vibrational-mode optomechanical system, which consists of two vibrational modes optomechanically coupled to a common cavity-field mode. We also analyze the dark-mode effect and its breaking in this system.

A. The Langevin equations

The Hamiltonian of the physical system considered in the main text reads (with $\hbar = 1$):

$$\mathcal{H} = \omega_c c^\dagger c + \sum_{j=1}^2 [\omega_j d_j^\dagger d_j + g_j c^\dagger c (d_j + d_j^\dagger)] + (\Omega c e^{i\omega_L t} + \Omega^* c^\dagger e^{-i\omega_L t}) + \mathcal{H}_\chi, \quad (\text{S1a})$$

$$\mathcal{H}_\chi = \chi (e^{i\Theta} d_1^\dagger d_2 + e^{-i\Theta} d_2^\dagger d_1), \quad (\text{S1b})$$

where c^\dagger (c) and d_j^\dagger (d_j) are the creation (annihilation) operators of the cavity-field mode (with resonance frequency ω_c) and the j th vibrational mode (with resonance frequency ω_j), respectively. The optomechanical interactions between the optical mode and the two vibrational modes are described by the radiation-pressure g_j terms. The Ω term describes cavity-field driving with driving frequency ω_L . The term \mathcal{H}_χ describes a phase-dependent phonon-hopping interaction between the two vibrations, which is introduced to break the dark mode in this system. In a rotating frame, defined by the unitary transformation operator $\exp(-i\omega_L c^\dagger c t)$, the Hamiltonian of the system becomes

$$\mathcal{H}_I = \Delta_c c^\dagger c + \sum_{j=1}^2 [\omega_j d_j^\dagger d_j + g_j c^\dagger c (d_j + d_j^\dagger)] + (\Omega c + \Omega^* c^\dagger) + \chi (e^{i\Theta} d_1^\dagger d_2 + e^{-i\Theta} d_2^\dagger d_1), \quad (\text{S2})$$

where $\Delta_c = \omega_c - \omega_L$ is the cavity-field driving detuning.

By phenomenologically adding the dissipation and noise terms into the Heisenberg equations, the quantum Langevin equations of this system can be obtained as:

*Electronic address: jqliao@hunnu.edu.cn

$$\begin{aligned}
\dot{c} &= -\left\{\kappa + i[\Delta_c + g_1(d_1 + d_1^\dagger) + g_2(d_2 + d_2^\dagger)]\right\}c - i\Omega^* + \sqrt{2\kappa}c_{\text{in}}, \\
\dot{d}_1 &= -(\gamma_1 + i\omega_1)d_1 - ig_1c^\dagger c - i\chi e^{i\Theta}d_2 + \sqrt{2\gamma_1}d_{1,\text{in}}, \\
\dot{d}_2 &= -(\gamma_2 + i\omega_2)d_2 - ig_2c^\dagger c - i\chi e^{-i\Theta}d_1 + \sqrt{2\gamma_2}d_{2,\text{in}},
\end{aligned} \tag{S3}$$

where κ ($\gamma_{j=1,2}$) is the decay rate of the optical (j th vibrational) mode, while c_{in} and $d_{j,\text{in}}$ are, respectively, the zero-mean input noise operators for the optical mode and the j th mechanical mode, characterized by the following correlation functions:

$$\begin{aligned}
\langle c_{\text{in}}(t)c_{\text{in}}^\dagger(t') \rangle &= \delta(t-t'), & \langle c_{\text{in}}^\dagger(t)c_{\text{in}}(t') \rangle &= 0, \\
\langle d_{j,\text{in}}(t)d_{j,\text{in}}^\dagger(t') \rangle &= (\bar{n}_j + 1)\delta(t-t'), & \langle d_{j,\text{in}}^\dagger(t)d_{j,\text{in}}(t') \rangle &= \bar{n}_j\delta(t-t'),
\end{aligned} \tag{S4}$$

where $\bar{n}_{j=1,2} = \{\exp[\hbar\omega_j/(k_B T_j)] - 1\}^{-1}$ denotes the average thermal occupation numbers associated with the heat bath of the j th mechanical mode, with k_B being the Boltzmann constant and T_j being the bath temperature of the j th mechanical mode.

By considering the strong-driving regime of the cavity, we can apply a linearization procedure to simplify the physical model. Specifically, we express the operators in Eqs. (S3) as the sum of their steady-state mean values and quantum fluctuations, i.e.,

$$o = \langle o \rangle_{\text{ss}} + \delta o \tag{S5}$$

for the operators $o \in \{c, c^\dagger, d_j, d_j^\dagger\}$.

By separating the classical motion and quantum fluctuations, the equations of motion for the classical-motion variables can be obtained as:

$$\begin{aligned}
\frac{d}{dt} \langle c \rangle &= -\left\{\kappa + i\left[\Delta_c + g_1(\langle d_1 \rangle + \langle d_1^\dagger \rangle) + g_2(\langle d_2 \rangle + \langle d_2^\dagger \rangle)\right]\right\} \langle c \rangle - i\Omega^*, \\
\frac{d}{dt} \langle d_1 \rangle &= -i\omega_1 \langle d_1 \rangle - ig_1 \langle c^\dagger \rangle \langle c \rangle - i\chi e^{i\Theta} \langle d_2 \rangle - \gamma_1 \langle d_1 \rangle, \\
\frac{d}{dt} \langle d_2 \rangle &= -i\omega_2 \langle d_2 \rangle - ig_2 \langle c^\dagger \rangle \langle c \rangle - i\chi e^{-i\Theta} \langle d_1 \rangle - \gamma_2 \langle d_2 \rangle.
\end{aligned} \tag{S6}$$

In this work, we focus on the steady-state entanglement of the system. Then, the steady-state mean values of the dynamical variables are obtained as:

$$\langle c \rangle_{\text{ss}} = \frac{-i\Omega^*}{\kappa + i\Delta}, \quad \langle d_1 \rangle_{\text{ss}} = \frac{-i(g_1 |\langle c \rangle_{\text{ss}}|^2 + \chi e^{i\Theta} \langle d_2 \rangle_{\text{ss}})}{\gamma_1 + i\omega_1}, \quad \langle d_2 \rangle_{\text{ss}} = \frac{-i(g_2 |\langle c \rangle_{\text{ss}}|^2 + \chi e^{-i\Theta} \langle d_1 \rangle_{\text{ss}})}{\gamma_2 + i\omega_2}, \tag{S7}$$

where we introduce the normalized driving detuning $\Delta = \Delta_c + 2 \sum_{j=1}^2 g_j \text{Re}[\langle d_j \rangle_{\text{ss}}]$, with $\text{Re}[\langle d_j \rangle_{\text{ss}}]$ taking the real part of $\langle d_j \rangle_{\text{ss}}$.

The linearized equations of motion for these quantum fluctuations are given by

$$\begin{aligned}
\delta \dot{c} &= -(\kappa + i\Delta)\delta c - iG_1(\delta d_1 + \delta d_1^\dagger) - iG_2(\delta d_2 + \delta d_2^\dagger) + \sqrt{2\kappa}c_{\text{in}}, \\
\delta \dot{d}_1 &= -iG_1^* \delta c - (\gamma_1 + i\omega_1)\delta d_1 - i\chi e^{i\Theta} \delta d_2 - iG_1 \delta c^\dagger + \sqrt{2\gamma_1}d_{1,\text{in}}, \\
\delta \dot{d}_2 &= -iG_2^* \delta c - i\chi e^{-i\Theta} \delta d_1 - (\gamma_2 + i\omega_2)\delta d_2 - iG_2 \delta c^\dagger + \sqrt{2\gamma_2}d_{2,\text{in}},
\end{aligned} \tag{S8}$$

where δc (δc^\dagger) and $\delta d_{j=1,2}$ (δd_j^\dagger) are the fluctuation operators of the cavity-field mode and the j th vibrational mode, respectively. $G_{j=1,2} = g_j \langle c \rangle_{\text{ss}}$ is the linearized optomechanical-coupling strength between the cavity field and the j th vibrational mode. Note that in the following discussions $\langle c \rangle_{\text{ss}}$ is assumed to be real, which is accessible by choosing a proper driving amplitude Ω . This indicates that the linearized optomechanical-coupling strength G_j is real too.

Based on Eq. (S8), we know that these three bosonic modes are coupled to each other through bilinear-form interactions. Mathematically, we can infer an effective Hamiltonian to govern these bilinear interactions, which include both excitation-exchanging (beam-splitting-type) terms and the excitation-creating (two-mode-squeezing) terms. In our optomechanical entanglement scheme, the beam-splitting-type interactions between these bosonic modes are expected to dominate the linearized couplings in this system, and hence we can simplify the Hamiltonian of the system by applying the rotating-wave approximation (RWA). The linearized optomechanical Hamiltonian in the RWA takes the following form (discarding the noise terms)

$$H_{\text{RWA}} = \Delta \delta c^\dagger \delta c + \sum_{j=1}^2 [\omega_j \delta d_j^\dagger \delta d_j + G_j (\delta c \delta d_j^\dagger + \delta d_j \delta c^\dagger)] + \chi (e^{i\Theta} \delta d_1^\dagger \delta d_2 + e^{-i\Theta} \delta d_2^\dagger \delta d_1). \tag{S9}$$

Below, we analyze the dark-mode effect in this system based on the Hamiltonian H_{RWA} in Eq. (S9).

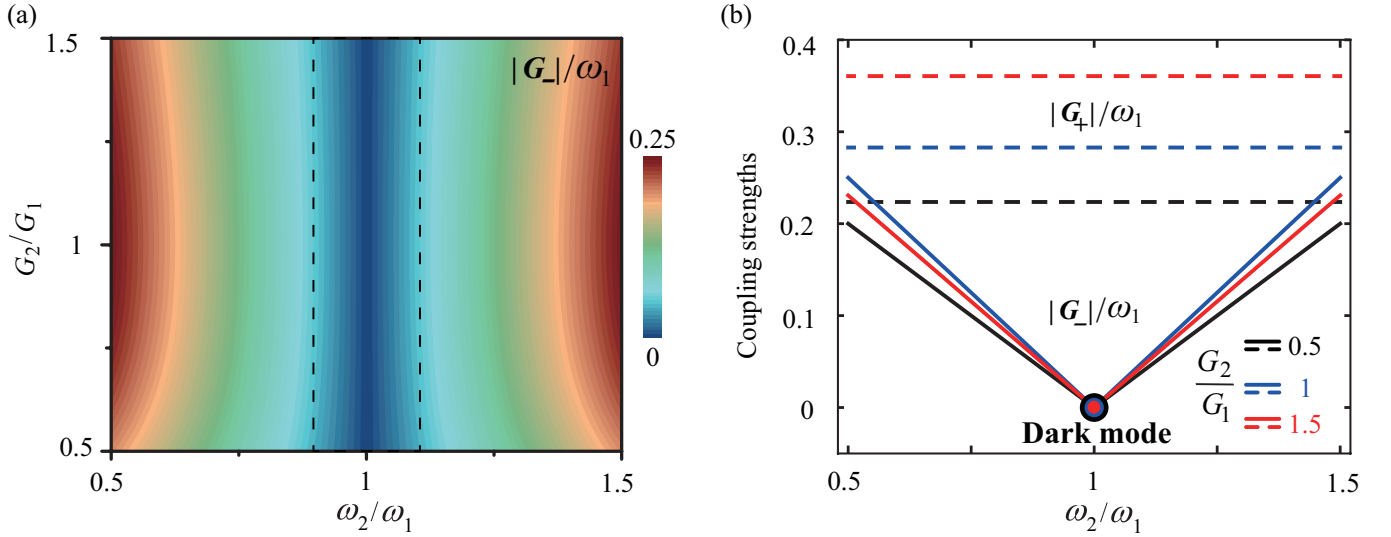


FIG. S1: (a) Coupling strength $|G_-|/\omega_1$ versus the frequency ratio ω_2/ω_1 and the coupling strength ratio G_2/G_1 of the two vibrational modes. (b) Coupling strengths $|G_+|/\omega_1$ (dashed lines) and $|G_-|/\omega_1$ (solid lines) versus the frequency ratio ω_2/ω_1 when $G_2/G_1=0.5$ (black lines), 1 (blue lines), and 1.5 (red lines). Here we set $G_1/\omega_1 = 0.2$.

B. Dark-mode effect

To study the dark-mode effect in this three-mode optomechanical system, we first consider the case where the synthetic magnetism (induced by the phonon-hopping term) is absent, i.e., dark-mode-unbreaking (DMU): $\chi = 0$, then the Hamiltonian (S9) is reduced to

$$H_{\text{RWA}} = \Delta \delta c^\dagger \delta c + \sum_{j=1}^2 [\omega_j \delta d_j^\dagger \delta d_j + G_j (\delta c \delta d_j^\dagger + \delta d_j \delta c^\dagger)]. \quad (\text{S10})$$

In this system, the two vibrational modes δd_1 and δd_2 coupled to a common optical mode δc form two hybrid mechanical modes, which are described by the two annihilation operators:

$$\mathcal{D}_+ = \frac{1}{\sqrt{G_1^2 + G_2^2}} (G_1 \delta d_1 + G_2 \delta d_2), \quad (\text{S11})$$

$$\mathcal{D}_- = \frac{1}{\sqrt{G_1^2 + G_2^2}} (G_2 \delta d_1 - G_1 \delta d_2). \quad (\text{S12})$$

It can be shown that the two hybrid vibrational modes satisfy the bosonic commutative relations $[\mathcal{D}_\pm, \mathcal{D}_\pm^\dagger] = 1$. The Hamiltonian in Eq. (S10) can be rewritten with the hybrid vibrational modes \mathcal{D}_+ and \mathcal{D}_- as

$$H_{\text{hyb}} = \Delta \delta c^\dagger \delta c + \omega_+ \mathcal{D}_+^\dagger \mathcal{D}_+ + \omega_- \mathcal{D}_-^\dagger \mathcal{D}_- + G_+ (\delta c \mathcal{D}_+^\dagger + \mathcal{D}_+ \delta c^\dagger) + G_- (\mathcal{D}_+^\dagger \mathcal{D}_- + \mathcal{D}_-^\dagger \mathcal{D}_+), \quad (\text{S13})$$

where we introduce the resonance frequencies ω_\pm and the coupling strengths G_\pm as:

$$\omega_+ = \frac{G_1^2 \omega_1 + G_2^2 \omega_2}{G_1^2 + G_2^2}, \quad \omega_- = \frac{G_2^2 \omega_1 + G_1^2 \omega_2}{G_1^2 + G_2^2}, \quad (\text{S14a})$$

$$G_+ = \sqrt{G_1^2 + G_2^2}, \quad G_- = \frac{G_1 G_2 (\omega_1 - \omega_2)}{G_1^2 + G_2^2}. \quad (\text{S14b})$$

We can see from Eqs. (S13) and (S14b) that, when $\omega_1 = \omega_2$, the mode \mathcal{D}_- is decoupled from the system (i.e., $G_- = 0$), so it is a dark mode, while \mathcal{D}_+ is a bright mode and it always couples to the cavity field due to $G_+ > 0$.

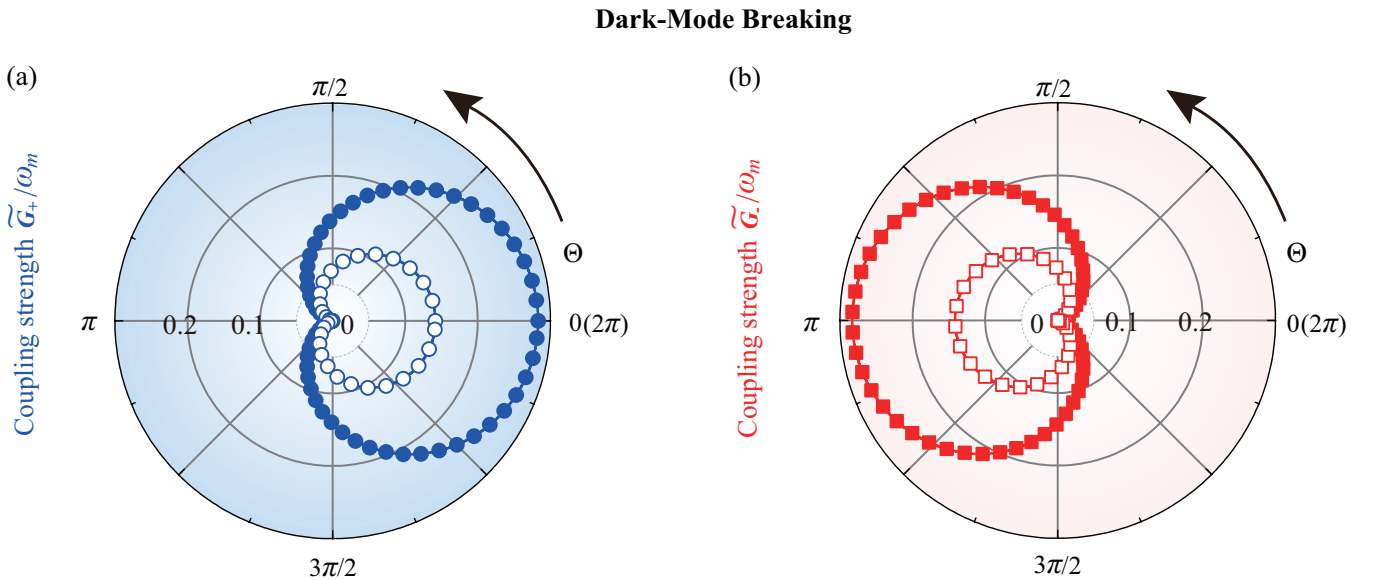


FIG. S2: Polar-coordinate representations of: (a) the redefined coupling strength \tilde{G}_+/ω_m versus the modulation phase Θ when $G_j/\omega_m = 0.1$ (blue hollow disks) and $G_j/\omega_m = 0.2$ (blue solid disks) for $j = 1, 2$; (b) the redefined coupling strength \tilde{G}_-/ω_m versus the modulation phase Θ when $G_j/\omega_m = 0.1$ (red hollow rectangles) and $G_j/\omega_m = 0.2$ (red solid rectangles). Here we have chosen the mechanical resonance frequency ω_m as the frequency scale and assumed $\chi/\omega_m = 0.1$ and $\omega_j/\omega_m = 1$.

In Fig. S1(a), we plot the redefined coupling strength $|G_-|/\omega_1$ as functions of the frequency ratio ω_2/ω_1 and the coupling-strength ratio G_2/G_1 of the two mechanical modes. We find that when $\omega_2 = \omega_1$, the redefined coupling strength G_- becomes zero, which indicates that the dark mode (i.e., the mode \mathcal{D}_-) emerges in the system. Though the dark mode exists theoretically only at $\omega_1 = \omega_2$, the dark-mode effect actually works for a wider detuning range [as marked by the dashed-line area in Fig. S1(a)]. Physically, the width of the dashed-line area is determined by the spectral resolution in the two-vibrational-mode optomechanical system. Here, this width is approximately determined by the cavity-field decay rate, because the decay rate of the vibrational mode is much smaller than that of the cavity field.

Owing to the existence of the dark-mode effect [S1–S6], the generation of quantum entanglement is completely suppressed in the three-mode optomechanical system. Physically, the two vibrational modes coupled to a common cavity-field mode can be hybridized into a bright mode and a dark mode. Here, the dark mode is decoupled from the system. As a result, the thermal excitations associated with the dark mode are kept in this system, and then the thermal noises associated with the dark mode destroy quantum entanglement. Thus, it is naturally to ask the question whether we can generate quantum entanglement by breaking the dark-mode effect in this optomechanical system.

C. Dark-mode breaking

To break the dark-mode effect in the two-vibrational-mode optomechanical system, a phase-dependent phonon-exchange interaction is introduced into the system, i.e., dark-mode-breaking (DMB) by assuming $\chi \neq 0$ and $\Theta \neq n\pi$. This phonon-hopping-coupling term is used to form a phase-dependent loop-coupled configuration and to generate an effective synthetic magnetism [S7–S15], which induces a path interference between two excitation-transport channels. Physically, the dark-mode effect can be broken by tuning the synthetic magnetism in this phase-dependent loop-coupled three-mode optomechanical system.

To induce the dark-mode breaking, we introduce two superposition-vibrational modes associated with the synthetic magnetism: $\tilde{\mathcal{D}}_+$ and $\tilde{\mathcal{D}}_-$, defined by:

$$\tilde{\mathcal{D}}_+ = \mathcal{F}\delta d_1 - e^{i\Theta}\mathcal{K}\delta d_2, \quad \tilde{\mathcal{D}}_- = e^{-i\Theta}\mathcal{K}\delta d_1 + \mathcal{F}\delta d_2, \quad (\text{S15})$$

then the Hamiltonian in Eq. (S9) becomes

$$H_{\text{RWA}} = \Delta\delta c^\dagger\delta c + \tilde{\omega}_+\tilde{\mathcal{D}}_+^\dagger\tilde{\mathcal{D}}_+ + \tilde{\omega}_-\tilde{\mathcal{D}}_-^\dagger\tilde{\mathcal{D}}_- + (\tilde{G}_+^*\delta c\tilde{\mathcal{D}}_+^\dagger + \tilde{G}_+\tilde{\mathcal{D}}_+\delta c^\dagger) + (\tilde{G}_-^*\delta c\tilde{\mathcal{D}}_-^\dagger + \tilde{G}_-\tilde{\mathcal{D}}_-\delta c^\dagger), \quad (\text{S16})$$

where the resonance frequencies $\tilde{\omega}_\pm$ and the coupling strengths \tilde{G}_\pm are defined as:

$$\tilde{\omega}_\pm = \frac{1}{2}(\omega_1 + \omega_2 \pm \sqrt{(\omega_1 - \omega_2)^2 + 4\chi^2}), \quad (\text{S17})$$

and

$$\tilde{G}_+ = \mathcal{F}G_1 - e^{-i\Theta}\mathcal{K}G_2, \quad \tilde{G}_- = e^{i\Theta}\mathcal{K}G_1 + \mathcal{F}G_2, \quad (\text{S18})$$

with

$$\mathcal{F} = |\tilde{\omega}_- - \omega_1|/\sqrt{(\tilde{\omega}_- - \omega_1)^2 + \chi^2}, \quad \mathcal{K} = \chi\mathcal{F}/(\tilde{\omega}_- - \omega_1). \quad (\text{S19})$$

In the degenerate-two-resonator case: $\omega_1 = \omega_2 = \omega_m$, the above introduced parameters become $\tilde{\omega}_\pm = \omega_m \pm \chi$, $\mathcal{F} = 1/\sqrt{2}$, and $\mathcal{K} = -1/\sqrt{2}$. Then the coupling strengths in Eq. (S18) can be simplified to

$$\tilde{G}_+ = (G_1 + e^{-i\Theta}G_2)/\sqrt{2}, \quad \tilde{G}_- = (G_2 - e^{i\Theta}G_1)/\sqrt{2}. \quad (\text{S20})$$

We proceed to analyze the dependence of the dark-mode effect on the real and positive coupling strengths G_1 and G_2 . Here, we consider the symmetric-coupling ($G_1 = G_2 = G$) case, and obtain the relations:

$$\tilde{G}_+ = G(1 + e^{-i\Theta})/\sqrt{2}, \quad \tilde{G}_- = G(1 - e^{i\Theta})/\sqrt{2}. \quad (\text{S21})$$

It can be seen from Eq. (S21) that, when $\Theta = n\pi$ for an integer n , one (i.e., the dark mode) of the two hybrid mechanical modes is decoupled from the cavity-field mode. In Figs. S2(a) and S2(b), we plot \tilde{G}_\pm as a function of Θ , when $\omega_1 = \omega_2$ and $G_1 = G_2$. We can see that the dark mode exists only when $\Theta = n\pi$. For an odd n , we obtain $\tilde{G}_+ = 0$ (see blue symbols), and thus \tilde{D}_+ becomes a dark mode. For an even n , we obtain $\tilde{G}_- = 0$ (see red symbols), and thus \tilde{D}_- becomes a dark mode. Tuning $\Theta \neq n\pi$ leads to an effective coupling of the dark mode to the optical mode, which indicates dark-mode breaking. Physically, a reconfigurable synthetic gauge field can be realized by tuning the phase Θ , which enables flexible switching between the DMU and DMB regimes.

Here we should highlight that we have performed the rotating-wave approximation (RWA) in the optomechanical interaction *only* in the derivation of the analytical expression of the dark mode, i.e., only in analytically demonstrating the dark-mode effect and its breaking. In other Sections of the main text and SM, we do not perform the RWA in the light-vibration coupling. In particular, in the derivation of the entanglement measures and numerical simulations, we considered *both* beam-splitter-type (rotating-wave terms) *and* two-mode-squeezing-type (counter-rotating terms) optomechanical interactions to study the generation of optomechanical entanglement.

II. GENERATING BIPARTITE OPTOMECHANICAL ENTANGLEMENT AND FULL TRIPARTITE OPTOMECHANICAL INSEPARABILITY VIA DARK-MODE BREAKING

In this section, we derive the steady-state variance matrix, and adopt the logarithmic negativity and the residual contangle to quantify bipartite entanglement and full tripartite inseparability in this system, respectively.

A. Steady-state variance matrix

By defining the optical and mechanical quadratures and the corresponding Hermitian input noise operators:

$$\begin{aligned} \delta X_o &= (\delta o^\dagger + \delta o)/\sqrt{2}, & \delta Y_o &= i(\delta o^\dagger - \delta o)/\sqrt{2}, \\ X_o^{\text{in}} &= (\delta o_{\text{in}}^\dagger + \delta o_{\text{in}})/\sqrt{2}, & Y_o^{\text{in}} &= i(\delta o_{\text{in}}^\dagger - \delta o_{\text{in}})/\sqrt{2}, \end{aligned} \quad (\text{S22})$$

the linearized Langevin equations in (S8) can be reexpressed as:

$$\begin{aligned} \delta \dot{X}_{d_1} &= -\gamma_1 \delta X_{d_1} + \omega_1 \delta Y_{d_1} + \chi(\sin \Theta \delta X_{d_2} + \cos \Theta \delta Y_{d_2}) + \sqrt{2\gamma_1} X_{d,1}^{\text{in}}, \\ \delta \dot{Y}_{d_1} &= -\omega_1 \delta X_{d_1} - \gamma_1 \delta Y_{d_1} - \chi(\cos \Theta \delta X_{d_2} - \sin \Theta \delta Y_{d_2}) - 2G_1 \delta X_c + \sqrt{2\gamma_1} Y_{d,1}^{\text{in}}, \\ \delta \dot{X}_{d_2} &= -\chi(\sin \Theta \delta X_{d_1} - \cos \Theta \delta Y_{d_1}) - \gamma_2 \delta X_{d_2} + \omega_2 \delta Y_{d_2} + \sqrt{2\gamma_2} X_{d,2}^{\text{in}}, \\ \delta \dot{Y}_{d_2} &= -\chi(\cos \Theta \delta X_{d_1} + \sin \Theta \delta Y_{d_1}) - \omega_2 \delta X_{d_2} - \gamma_2 \delta Y_{d_2} - 2G_2 \delta X_c + \sqrt{2\gamma_2} Y_{d,2}^{\text{in}}, \\ \delta \dot{X}_c &= -\kappa \delta X_c + \Delta \delta Y_c + \sqrt{2\kappa} X_c^{\text{in}}, \\ \delta \dot{Y}_c &= -2G_1 \delta X_{d_1} - 2G_2 \delta X_{d_2} - \Delta \delta X_c - \kappa \delta Y_c + \sqrt{2\kappa} Y_c^{\text{in}}. \end{aligned} \quad (\text{S23})$$

The Langevin equations (S23) can be reexpressed as a compact form:

$$\dot{\mathbf{u}}(t) = \mathbf{A}\mathbf{u}(t) + \mathbf{N}(t), \quad (\text{S24})$$

where we introduce the fluctuation operator vector

$$\mathbf{u}(t) = [\delta X_{d_1}, \delta Y_{d_1}, \delta X_{d_2}, \delta Y_{d_2}, \delta X_c, \delta Y_c]^T, \quad (\text{S25})$$

the noise operator vector

$$\mathbf{N}(t) = \sqrt{2}[\sqrt{\gamma_1}X_{d_1}^{\text{in}}, \sqrt{\gamma_1}Y_{d_1}^{\text{in}}, \sqrt{\gamma_2}X_{d_2}^{\text{in}}, \sqrt{\gamma_2}Y_{d_2}^{\text{in}}, \sqrt{\kappa}X_c^{\text{in}}, \sqrt{\kappa}Y_c^{\text{in}}]^T, \quad (\text{S26})$$

and the coefficient matrix

$$\mathbf{A} = \begin{pmatrix} -\gamma_1 & \omega_1 & \chi_+ & \chi_- & 0 & 0 \\ -\omega_1 & -\gamma_1 & -\chi_- & \chi_+ & -2G_1 & 0 \\ -\chi_+ & \chi_- & -\gamma_2 & \omega_2 & 0 & 0 \\ -\chi_- & -\chi_+ & -\omega_2 & -\gamma_2 & -2G_2 & 0 \\ 0 & 0 & 0 & 0 & -\kappa & \Delta \\ -2G_1 & 0 & -2G_2 & 0 & -\Delta & -\kappa \end{pmatrix}, \quad (\text{S27})$$

with $\chi_+ = \chi \sin \Theta$ and $\chi_- = \chi \cos \Theta$. A formal solution of the linearized Langevin equation (S24) is given by

$$\mathbf{u}(t) = \mathbf{M}(t)\mathbf{u}(0) + \int_0^t \mathbf{M}(t-s)\mathbf{N}(s)ds, \quad (\text{S28})$$

where $\mathbf{M}(t) = \exp(\mathbf{A}t)$. Note that the parameters chosen for all our numerical simulations satisfy the stability conditions derived from the Routh-Hurwitz criterion [S16]. Namely, the real parts of all the eigenvalues of \mathbf{A} are negative.

For studying the quantum entanglement between the optical mode and the mechanical modes, we calculate the steady-state value of the covariance matrix \mathbf{V} , which is defined by the matrix elements

$$\mathbf{V}_{kl} = \frac{1}{2}[\langle \mathbf{u}_k(\infty)\mathbf{u}_l(\infty) \rangle + \langle \mathbf{u}_l(\infty)\mathbf{u}_k(\infty) \rangle], \quad (\text{S29})$$

for $k, l = 1-6$. Under the stability condition, the steady-state covariance matrix \mathbf{V} fulfills the Lyapunov equation,

$$\mathbf{A}\mathbf{V} + \mathbf{V}\mathbf{A}^T = -\mathbf{Q}, \quad (\text{S30})$$

where we introduce the matrix

$$\mathbf{Q} = \frac{1}{2}(\mathbf{C} + \mathbf{C}^T), \quad (\text{S31})$$

with \mathbf{C} being the noise correlation matrix, which can be defined through the matrix elements,

$$\langle \mathbf{N}_k(s)\mathbf{N}_l(s') \rangle = \mathbf{C}_{k,l}\delta(s-s'). \quad (\text{S32})$$

In terms of Eqs. (S26), (S31), and (S32), the expression of the matrix \mathbf{Q} can be obtained as

$$\mathbf{Q} = \text{diag}\{\gamma_1(2\bar{n}_1 + 1), \gamma_1(2\bar{n}_1 + 1), \gamma_2(2\bar{n}_2 + 1), \gamma_2(2\bar{n}_2 + 1), \kappa, \kappa\}. \quad (\text{S33})$$

Based on Eqs. (S27), (S30), and (S33), we can obtain the steady-state variance matrix \mathbf{V} . Then, the steady-state properties of the three-mode optomechanical system can be achieved.

B. Bipartite entanglement and full tripartite inseparability measures

Here, we apply two entanglement measures: the logarithmic negativity and minimum residual contangle, which are used to quantify the bipartite entanglement and full tripartite inseparability, respectively.

1. Logarithmic negativity

The optomechanical entanglement between the optical mode and the j th vibrational mode can be quantified using the logarithmic negativity $E_{\mathcal{N},j}$, defined as [S17]

$$E_{\mathcal{N},j} \equiv \max\left[0, -\ln(2\zeta_j^-)\right], \quad (\text{S34})$$

where

$$\zeta_j^- \equiv 2^{-1/2}\{\Sigma(\mathbf{V}'_j) - [\Sigma(\mathbf{V}'_j)^2 - 4\det\mathbf{V}'_j]^{1/2}\}^{1/2}, \quad (\text{S35})$$

with

$$\Sigma(\mathbf{V}'_j) \equiv \det\mathcal{A}_j + \det\mathcal{B} - 2\det C_j, \quad (\text{S36})$$

being the smallest eigenvalue of the partial transpose of the reduced correlation matrix \mathbf{V}'_j . In Eq. (S35), the reduced correlation matrices \mathbf{V}'_j is obtained by removing the rows and columns of the uninteresting mode in \mathbf{V} . The matrix \mathbf{V}'_j takes the form as

$$\mathbf{V}'_j = \begin{pmatrix} \mathcal{A}_j & C_j \\ C_j^T & \mathcal{B} \end{pmatrix}, \quad (\text{S37})$$

where \mathcal{A}_j , \mathcal{B} , and C_j are 2×2 subblock matrices of \mathbf{V}'_j .

2. Minimum residual contangle

To study the full tripartite optomechanical inseparability in the three-mode optomechanical system, we apply a quantitative measure of the residual contangle \bar{E}_τ^{rst} [S18–S21], which is given by

$$\bar{E}_\tau^{rst} \equiv E_\tau^{r(st)} - E_\tau^{rs} - E_\tau^{rt}, \quad r, s, t \in \{d_1, d_2, c\}, \quad (\text{S38})$$

where E_τ^{uv} denotes the contangle of subsystems of u (u contains only one mode) and v (v contains one or two modes), and (r, s, t) denotes all the permutations of the three mode indexes [S18]. E_τ^{uv} is a proper entanglement monotone, and it can be defined as the squared logarithmic negativity [S18]

$$E_\tau^{uv} \equiv [E_{\mathcal{N}}]^2 \equiv \left\{ \max[0, -\ln(2\tilde{\nu}_-)] \right\}^2, \quad (\text{S39})$$

where $\tilde{\nu}_-$ is the minimum symplectic eigenvalue of the covariance matrix.

(i) When v contains only one mode, $\tilde{\nu}_-$ in Eq. (S39) is given by

$$\tilde{\nu}_- = \min\left[\text{eig}|i\Omega_2\tilde{\mathbf{V}}_4|\right], \quad (\text{S40})$$

where

$$\Omega_2 = \bigoplus_{j=1}^2 i\sigma_y, \quad (\text{S41})$$

with σ_y being the y -direction Pauli matrix. The matrix \mathbf{V}_4 in Eq. (S40) is defined by

$$\tilde{\mathbf{V}}_4 = P_0\mathbf{V}_4P_0, \quad (\text{S42})$$

where \mathbf{V}_4 is the 4×4 covariance matrix of two subsystems, obtained by removing the rows and columns of the uninteresting mode in \mathbf{V} , and

$$P_0 = \text{diag}(1, -1, 1, 1) \quad (\text{S43})$$

denotes the matrix that realizes the partial transposition at the level of the covariance matrixes.

(ii) When ν contains two modes, $\tilde{\nu}_-$ in Eq. (S39) is given by

$$\tilde{\nu}_- = \min \left[\text{eig} [i\Omega_3 \tilde{\mathbf{V}}] \right], \quad (\text{S44})$$

where

$$\Omega_3 = \bigoplus_{j=1}^3 i\sigma_y, \quad (\text{S45})$$

and

$$\tilde{\mathbf{V}} = P_{r(st)} \mathbf{V} P_{r(st)}. \quad (\text{S46})$$

Here, \mathbf{V} is the 6×6 covariance matrix of the system, and we introduce the partial transposition matrices

$$\begin{aligned} P_{d_1(d_2c)} &= \text{diag}(1, -1, 1, 1, 1, 1), \\ P_{d_2(d_1c)} &= \text{diag}(1, 1, 1, -1, 1, 1), \\ P_{c(d_1d_2)} &= \text{diag}(1, 1, 1, 1, 1, -1). \end{aligned} \quad (\text{S47})$$

The residual contangle satisfies the monogamy of quantum entanglement, i.e.,

$$E_\tau^{r(st)} \geq E_\tau^{rs} + E_\tau^{rt}. \quad (\text{S48})$$

This inequality is similar to the Coffman-Kundu-Wootters monogamy inequality, which holds for three qubits [S20].

A quantification of the continuous-variable tripartite inseparability is provided by the minimum residual contangle [S18]

$$E_\tau^{r|st} \equiv \min_{(r,s,t)} [E_\tau^{r(st)} - E_\tau^{rs} - E_\tau^{rt}], \quad (\text{S49})$$

where $(r, s, t \in \{d_1, d_2, c\})$ denotes all the permutations of the three mode indexes [S18]. The nonzero minimum residual contangle $E_\tau^{r|st} > 0$ means that the full tripartite inseparability is generated.

C. Optomechanical entanglement

When the two mechanical modes are coupled to a common optical mode, the two mechanical modes can form two hybrid mechanical modes: a dark mode and a bright mode. The dark mode is decoupled from both the bright mode and the cavity-field mode. As a result, the quantum entanglement of light and motion is generally destroyed by thermal noise concealed in the dark mode. To break the dark-mode effect, we introduce a phase-dependent phonon-exchange interaction between the two vibrational modes to build a loop-coupled configuration, and thus an effective synthetic magnetism can be induced in this phase-dependent loop-coupled system. In this section, we study the optomechanical entanglement in the three-mode optomechanical system. Concretely, we consider both the degenerate and non-degenerate mechanical mode cases. We focus on quantum entanglement in both the dark-mode-breaking and dark-mode-unbreaking regimes. By analyzing the optomechanical entanglement in the cases of both the presence and the absence of the dark modes, we can confirm the action of the dark-mode breaking on the enhancement of the entanglement.

1. Degenerate-mechanical-mode case

We first study optomechanical entanglement in the degenerate-mechanical-mode case. The introduced synthetic magnetism plays a critical role in the creation of light-vibration entanglement. Below, we study how synthetic magnetism affects the generation of light-vibration entanglement, i.e., we study the dependence of the light-vibration entanglement on the parameters Θ and χ of the phase-dependent phonon-exchange coupling.

In Figs. S3(a) and S3(b), we plot the light-vibration entanglement measure $E_{N,j}$ as functions of the modulation phase Θ and the effective driving detuning Δ when the system operates in the DMB regime. We can see that there exist two red holes in each figure around $\Delta = \omega_m$, which indicate that the photon-phonon entanglement can be created around the red-sideband resonance. In particular, the optomechanical entanglement $E_{N,1}$ ($E_{N,2}$) is much larger than $E_{N,2}$ ($E_{N,1}$) in the region $0 < \Theta < \pi$ ($\pi < \Theta < 2\pi$). This is because the synthetic magnetism enabled in the loop-coupled system can be modulated by tuning Θ . The maximal entanglement emerges at $\Theta = \pi/2$ and $3\pi/2$, corresponding to a strong path interference between two excitation-transport channels.

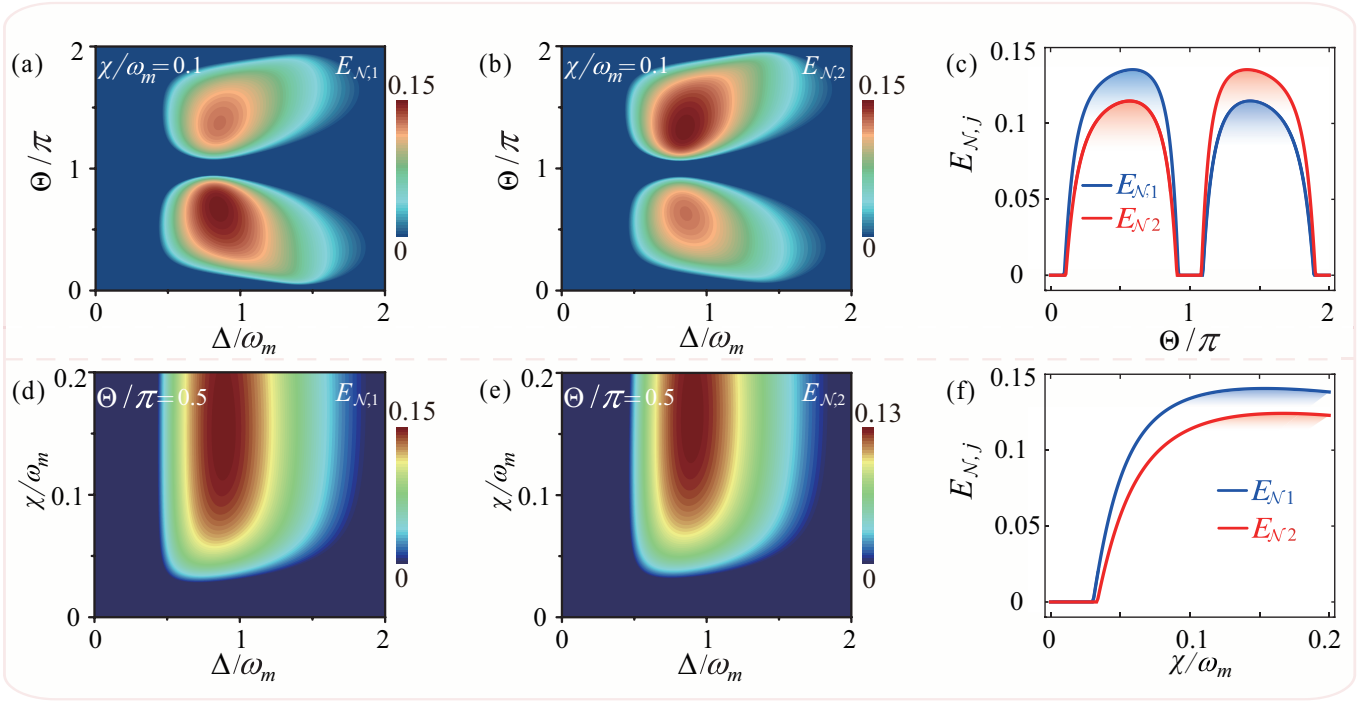


FIG. S3: (a,b) Logarithmic negativity $E_{N,j}$, quantifying quantum entanglement between the optical mode and the j th vibrational mode, versus the modulation phase Θ and the effective driving detuning Δ in the DMB regime, when the phonon-hopping coupling strength $\chi/\omega_m = 0.1$. (c) $E_{N,1}$ (blue curve) and $E_{N,2}$ (red curve) versus Θ when $\chi/\omega_m = 0.1$. Logarithmic negativities (d) $E_{N,1}$ and (e) $E_{N,2}$ versus the effective driving detuning Δ and the phonon-exchange coupling strength χ , when the modulation phase $\Theta = \pi/2$. (f) $E_{N,1}$ (blue curve) and $E_{N,2}$ (red curve) versus χ when $\Theta = \pi/2$. In our simulations, we have chosen the mechanical resonance frequency ω_m as the frequency scale and assumed the experimentally feasible parameters: $\omega_j/\omega_m = 1$, $\gamma_j/\omega_m = 10^{-5}$, $G_j/\omega_m = 0.2$, $\kappa/\omega_m = 0.2$, and $\bar{n}_j = 100$ for $j = 1, 2$.

We can also see from Figs. S3(a) and S3(b) that, at proper values of the modulation phase Θ ($\Theta \neq n\pi$), the optimal photon-phonon entanglement locates around the red-sideband resonance, i.e., $\Delta = \omega_m$. Additionally, the optomechanical entanglement is completely destroyed, i.e., $E_{N,1} = E_{N,2} = 0$ at $\Theta = n\pi$ for an integer n , which corresponds to the emergence of the dark mode. Hence, it is possible to switch the device between separable and entangled states by tuning the synthetic magnetism (i.e., the modulation phase Θ).

In Figs. S3(d), S3(e), and S3(f), we find that, in the absence of the synthetic magnetism (i.e., $\chi = 0$), there is no optomechanical entanglement completely. This is because the system possesses the dark mode and the thermal noise stored in this dark mode destroys quantum entanglement. In contrast to this, when we introduce a proper synthetic magnetism ($\chi \neq 0$ and $\Theta \neq n\pi$), light and multiple vibrations become entangled owing to the breaking of the dark mode. Moreover, the maximal optomechanical entanglement can be observed at $\chi \approx 0.15\omega_m$ and the red-sideband resonance $\Delta = \omega_m$.

Though the dark mode exists theoretically only in the two-degenerate-resonator case ($\omega_1 = \omega_2$), the dark-mode effect is observed within a finite parameter range for $\omega_1 \neq \omega_2$ (i.e., the detuning window). Next, we show the dependence of the detuning-window width of the dark-mode effect on the thermal phonon numbers \bar{n} of the vibrational modes.

In Fig. S4, we plot $E_{N,1}$ and $E_{N,2}$ as functions of the frequency ratio ω_2/ω_1 and the thermal excitation numbers \bar{n} of the two mechanical modes in both the DMU [$\chi = 0$, see Figs. S4(a), S4(b), and S4(c)] and DMB [$\chi/\omega_1 = 0.1$ and $\Theta = \pi/2$, see Figs. S4(d), S4(e), and S4(f)] regimes. In the DMU regime, the optomechanical entanglement is suppressed in a wide frequency-detuning range, and the suppression range of quantum entanglement becomes much wider for a larger value of thermal phonon number \bar{n} , as marked by the dark blue area in Figs. S4(a) and S4(b). For example, Fig. S4(c) shows that the dark-mode effect is observed for a finite frequency-detuning range, and that the range for $\bar{n} = 300$ is wider than that for $\bar{n} = 100$. In the DMB regime, we can see that the light and vibrations are entangled irrespective of the value of the ratio ω_2/ω_1 for a wide range of \bar{n} , as shown in Figs. S4(d) and S4(e). These results confirm that light and vibrations can be entangled via the DMB mechanism even when light-vibration entanglement is fully destroyed in the DMU regime. By breaking the dark-mode effect with the synthetic magnetism, $E_{N,1}$ and $E_{N,2}$ can be switched from significantly suppressed, or even fully destroyed, to fully entangled [see Fig. S4(f)]. These results indicate that the introduced synthetic magnetism can be used for enhancing the optomechanical entanglement for both degenerate and nondegenerate mechanical resonators, and especially, the work window of the synthetic magnetism becomes wider for a larger value of the thermal phonon number of the mechanical resonator.

In addition, we find that in the nondegenerate-resonator case (i.e., $\omega_1 \neq \omega_2$), the optomechanical entanglement may be slightly

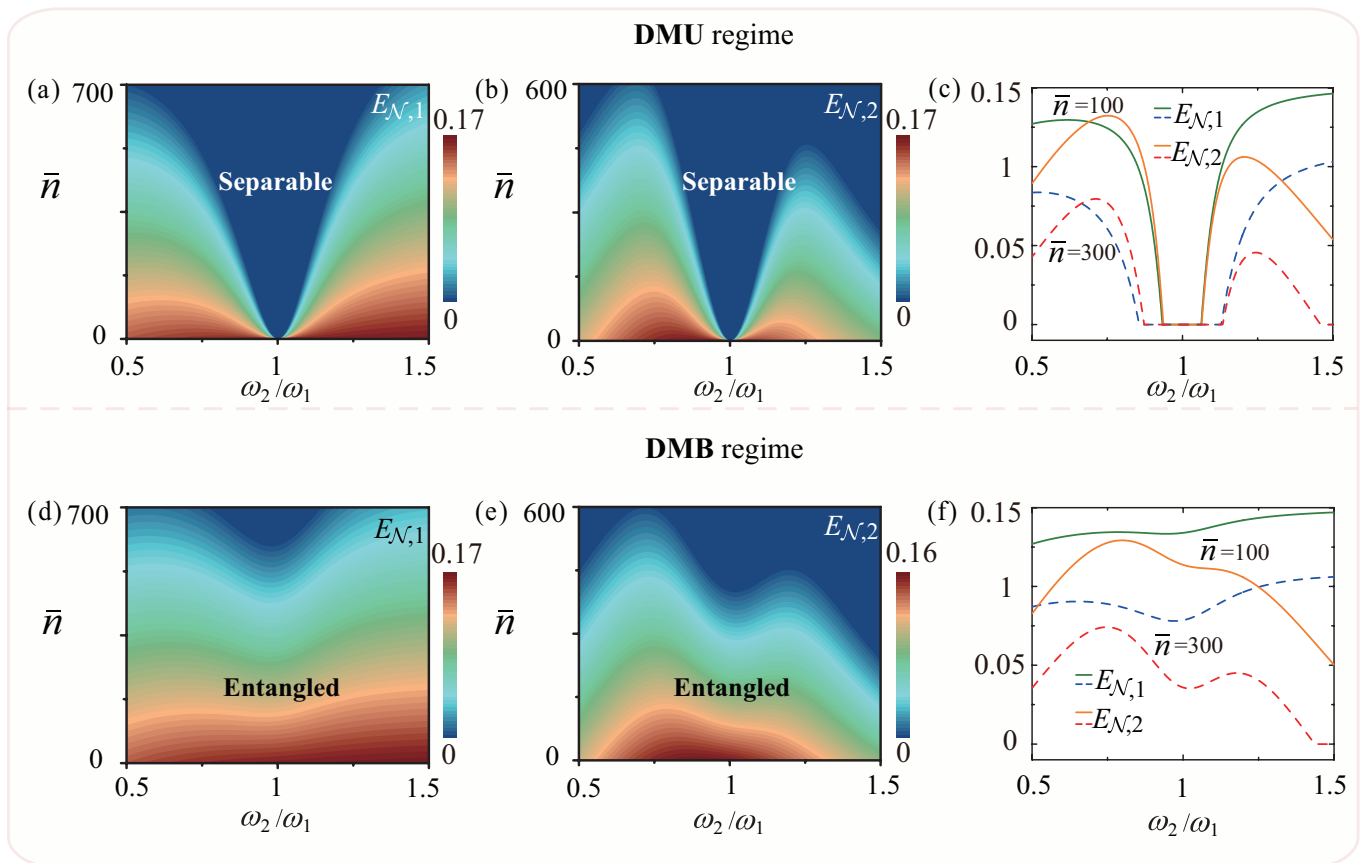


FIG. S4: Logarithmic negativities (a) $E_{N,1}$ and (b) $E_{N,2}$ versus the thermal phonon numbers $\bar{n}_j = \bar{n}$ and the resonance frequency ratio ω_2/ω_1 of the two mechanical modes in the DMU regime ($\chi = 0$). (c) $E_{N,1}$ and $E_{N,2}$ versus ω_2/ω_1 when $\bar{n} = 100$ (solid curves) and $\bar{n} = 300$ (dashed curves) in the DMU regime. (d) $E_{N,1}$ and (e) $E_{N,2}$ versus \bar{n} and ω_2/ω_1 in the DMB regime ($\chi/\omega_1 = 0.1$ and $\Theta = \pi/2$). (f) $E_{N,1}$ and $E_{N,2}$ versus ω_2/ω_1 when $\bar{n} = 100$ (solid curves) and $\bar{n} = 300$ (dashed curves) in the DMB regime. Other parameters used are the same as those in Fig. S3.

degraded by the introduced synthetic magnetism, as shown in Figs. S4(c) and S4(f). We explain this entanglement-degradation phenomenon based on two points: (i) The dark-mode effect exists within a frequency-detuning window, and therefore, within this window, the breaking of the dark-mode effect is the dominating factor for the entanglement-generation performance; (ii) Out of this window, the combination effect of the original optomechanical couplings and the introduced phase-dependent phonon-hopping interactions governs the entanglement generation, and hence the quantum interference effect induced by the two coupling channels can change the optomechanical entanglement through both constructive and destructive interferences.

Thermal noises in practical devices destroy fragile quantum resources. To protect quantum resources from environmental thermal perturbations, we introduce the synthetic magnetism which can significantly develop the noise tolerance of the quantum entanglement. To investigate the influence of the synthetic magnetism on the noise-tolerant quantum entanglement, we plot the logarithmic negativity $E_{N,j}$ as a function of the modulation phase Θ and the thermal excitations \bar{n} in the mechanical resonators, as shown in Fig. S5. We can see that, in the DMU regime, quantum entanglement emerges only when $\bar{n}_j \ll 1$; while in the DMB regime, it can persist to an extremely high thermal phonon numbers. In addition, we also have confirmed that the stronger synthetic magnetism leads to a larger noise-tolerant entanglement, which is generated via the DMB mechanism. This means that the DMB mechanism provides a feasible way to create and protect fragile quantum resources against dark modes, and build noise-tolerant quantum devices and entanglement switches.

In particular, quantum entanglement between light and multiple mechanical modes can be switched on and off on demand by engineering the synthetic magnetism. For example, when $0.5 < \bar{n}_j < 400$, both two entanglement channels are cut off due to the absence of the synthetic magnetism, while by inducing the synthetic magnetism, these channels are turned on simultaneously. The maximal synthetic magnetism (i.e., $\Theta = \pi/2$ and $3\pi/2$) leads to a strong entanglement. Additionally, we find that when $400 < \bar{n}_j < 700$, there exists only one entanglement channel, i.e., for $\Theta = \pi/2$ ($3\pi/2$), an optomechanical entanglement $E_{N,1}$ ($E_{N,2}$) is created, while no entanglement occurs for the other one. This indicates that a selective entanglement switch can be achieved.

We also study the influence of the cavity-field decay rate κ on the light-vibration entanglement when the system works in both

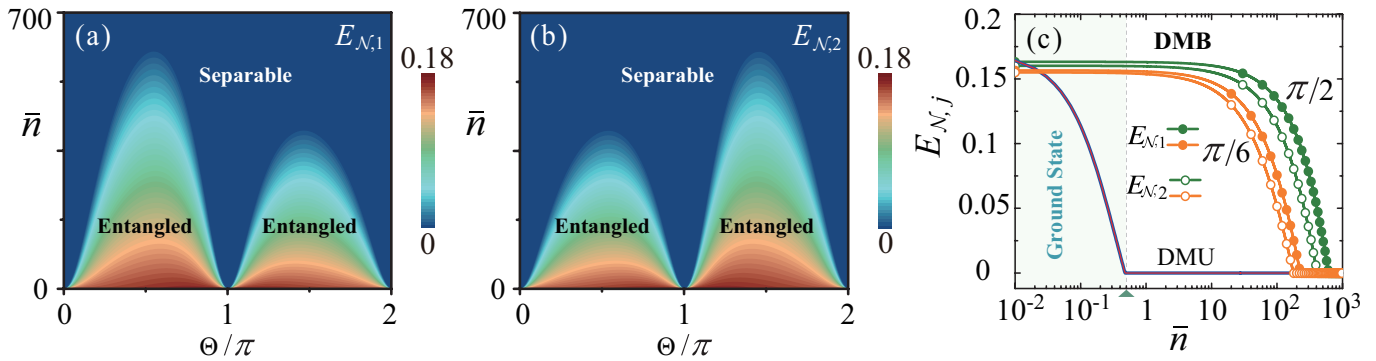


FIG. S5: Logarithmic negativities (a) $E_{N,1}$ and (b) $E_{N,2}$ versus the modulation phase Θ and the thermal phonon numbers \bar{n} of the two vibrational modes via the DMB mechanism. (c) $E_{N,1}$ and $E_{N,2}$ as functions of the thermal phonon numbers \bar{n} when $\Theta = \pi/6$ and $\Theta = \pi/2$ in both DMU (solid curves) and DMB (marked by symbols) regimes. Other parameters used are the same as those in Fig. S3.

DMB and DMU regimes. In Figs. S6(a) and S6(b), we plot the logarithmic negativity $E_{N,j}$ as a function of the rescaled cavity-field decay rate κ/ω_m when the system works in both the DMU and DMB regimes. Here, we can see that, in the DMU regime, the light and vibration are separable, i.e., $E_{N,j} = 0$ (see the solid lines). When switching to the DMB regime, optomechanical entanglement can be realized when the system is in the resolved-sideband regime, i.e., $\kappa \ll \omega_m$. The optimal working parameter of the cavity-field decay rate κ (corresponding to the maximum value of the logarithmic negativity $E_{N,j}$) is around $\kappa/\omega_m \approx 0.2$.

The vibrational modes are thermalized by their thermal baths through the mechanical dissipation channels, and thermal noises can destroy fragile quantum correlations in practical devices. Below, we study the dependence of the optomechanical entanglement on the mechanical decay rate γ_m .

In Figs. S6(c) and S6(d), we show the logarithmic negativity $E_{N,j}$ as a function of the mechanical decay rate γ_m , when the system operates in both the DMB (dashed lines) and DMU (solid lines) regimes. We can see that the values of the logarithmic negativity $E_{N,j}$ increase with the decrease of the mechanical decay rate γ_m . This is because the thermal-noise-exchange rates between the mechanical resonators and their heat baths are much slower for a smaller value of the decay rate γ_m , and it is good for protecting quantum resources from environmental thermal perturbations. This indicates that a high Q -factor resonator can be useful for generating a robust quantum entanglement. In Figs. S6(c) and S6(d), we have $E_{N,1} > E_{N,2}$ because the phase angle $\Theta = \pi/2$ is set, then quantum entanglement between the first mechanical mode and the cavity-field mode is stronger than that between the second mechanical mode and the optical mode. However, an opposite entanglement phenomenon, compared with the case of $\Theta = \pi/2$, emerges when $\Theta = 3\pi/2$, as shown in Figs. S6(c) and S6(d).

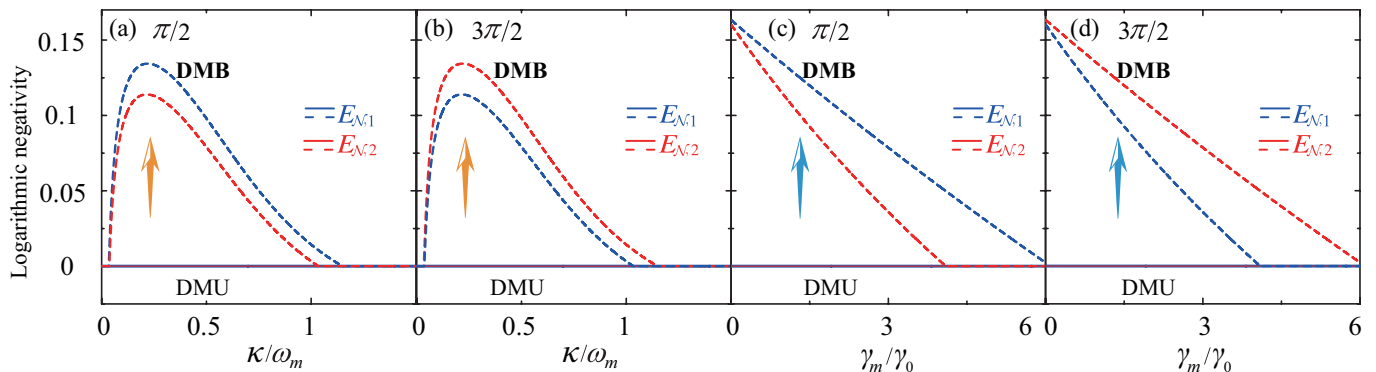


FIG. S6: (a,b) Logarithmic negativity $E_{N,j}$ versus the cavity-field decay rate κ when (a) $\Theta = \pi/2$ and (b) $\Theta = 3\pi/2$ in the DMB (dashed curves) regime. Here we assume $\gamma_m/\omega_m = 10^{-5}$. (c,d) Logarithmic negativity $E_{N,j}$ versus the mechanical dampings γ_m when (c) $\Theta = \pi/2$ and (d) $\Theta = 3\pi/2$ in the DMB (dashed curves) regime. Here we set $\kappa/\omega_m = 0.2$ and $\gamma_0/\omega_m = 10^{-5}$. Other parameters used are the same as those in Fig. S3. In these four cases, we also present the corresponding entanglement in the DMU regime (solid curves) for comparison with that in the DMB regime.

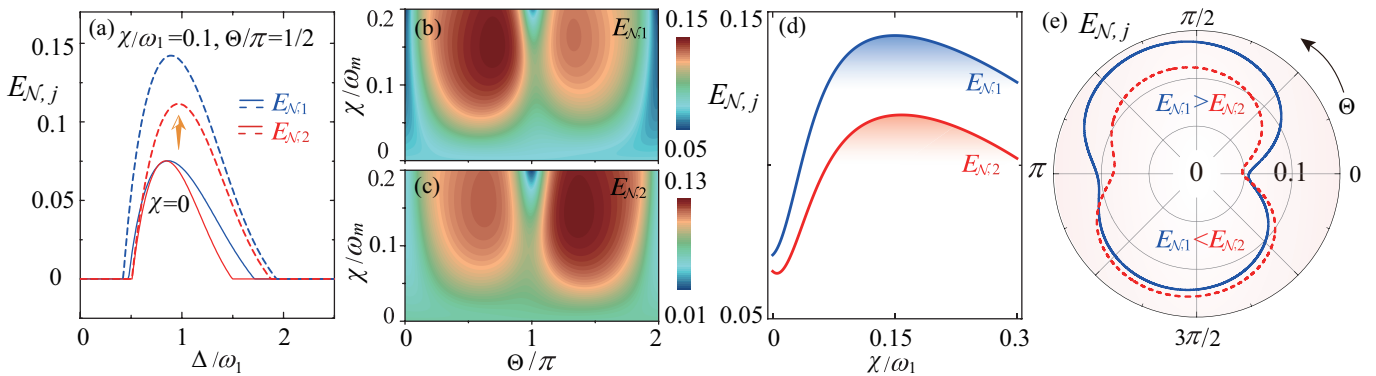


FIG. S7: (a) Logarithmic negativities $E_{N,1}$ (blue curves) and $E_{N,2}$ (red curves) between the optical mode and each mechanical mode versus the effective driving detuning Δ in various cases: $\chi = 0$ (solid curves), and $\chi = 0.1\omega_1$ and $\Theta = \pi/2$ (dashed curves). (b) $E_{N,1}$ and (c) $E_{N,2}$ versus χ and Θ , when $\Delta = \omega_1$. (d) $E_{N,1}$ (blue curve) and $E_{N,2}$ (red curve) vs χ , when $\Theta = \pi/2$. (e) $E_{N,1}$ (blue solid curve) and $E_{N,2}$ (red dashed curve) vs Θ in the polar coordinates, when $\chi = 0.1\omega_1$. Here we set $\omega_2 = 1.1\omega_1$, and other parameters are the same as those in Fig. S3.

2. Nondegenerate-vibrational-mode case

In the degenerate-vibrational-mode case, i.e., $\omega_1 = \omega_2$, the introduced phase-dependent phonon-hopping interaction is used to induce a synthetic magnetism and then control the dark-mode effect.

In the nondegenerate-vibrational-mode case, i.e., $\omega_1 \neq \omega_2$, though there is no dark mode, the synthetic magnetism can also be used for modulating the optomechanical entanglement. In this section, we study the dependence of the light-vibration entanglement on the synthetic magnetism in the nondegenerate-mechanical-mode case.

As an example, in a nondegenerate-mechanical-mode case of $\omega_2 = 1.1\omega_1$, we plot the logarithmic negativity $E_{N,j}$ of the optical mode and the j th mechanical mode as a function of the driving detuning Δ in the absence ($\chi = 0$, solid curves) and presence ($\chi = 0.1\omega_m$ and $\Theta = \pi/2$, dashed curves) of the synthetic magnetism, as shown in Fig. S7(a). It shows that light and vibrations are correlated in both cases: without the synthetic magnetism ($E_{N,1} = E_{N,2} = 0.07$, see the lower solid curves) and with the synthetic magnetism ($E_{N,1} = 0.15$, $E_{N,2} = 0.12$, see the upper dashed curves). In particular, the peak entanglement appears around the red-sideband resonance, i.e., $\Delta \approx \omega_1$. In principle, when the two mechanical resonators are far-off-resonant with each other, there is no dark mode, then quantum entanglement can be generated under a proper driving condition (the red-sideband resonance).

Since the phase-dependent phonon-hopping interaction (synthetic magnetism) plays a critical role in the enhancement of light-vibration entanglement, we investigate the dependence of the optomechanical entanglement on the parameters χ and Θ of the phase-dependent phonon-hopping coupling. In Fig. S7 (a), we plot the logarithmic negativity $E_{N,j}$ versus the parameters χ and Θ in the nondegenerate-vibrational-mode case. The plots show that the light-vibration entanglement in the nondegenerate-mechanical-resonator case can be controlled via the phase-dependent phonon-hopping interaction (i.e., the phase in a loop coupling leads to a synthetic magnetism). In particular, the optomechanical entanglement $E_{N,1}$ ($E_{N,2}$) is much larger than $E_{N,2}$

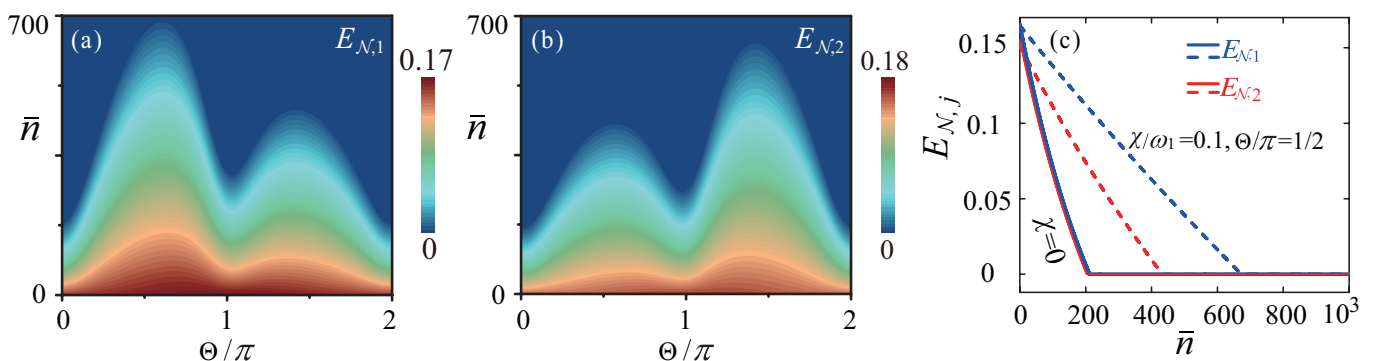


FIG. S8: Logarithmic negativities (a) $E_{N,1}$ and (b) $E_{N,2}$ versus the modulation phase Θ and the thermal phonon numbers \bar{n} when $\chi = 0.1\omega_1$ and $\Theta = \pi/2$. (c) $E_{N,1}$ (blue curves) and $E_{N,2}$ (red curves) as functions of the thermal phonon numbers \bar{n} when $\chi = 0$ (solid curves), and $\chi = 0.1\omega_1$ and $\Theta = \pi/2$ (dashed curves). Here we set $\omega_2 = 1.1\omega_1$, and other parameters are the same as those in Fig. S3.

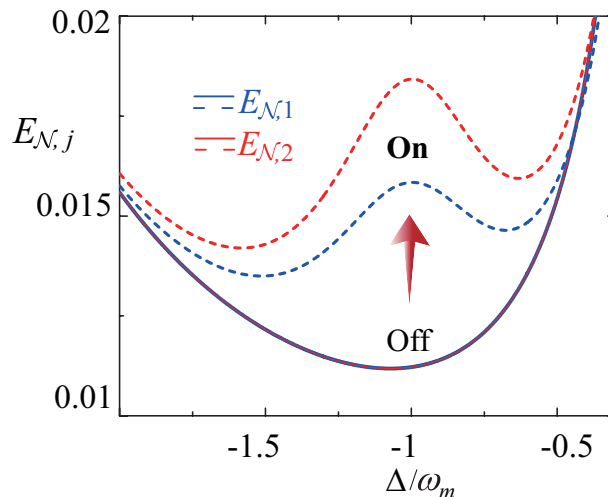


FIG. S9: Bipartite entanglement measures $E_{N,j=1,2}$ of the j th vibrational mode and the cavity-field mode versus Δ/ω_m when the synthetic magnetism is off ($\chi = 0$, the lower solid lines) and on ($\chi/\omega_m = 0.02$ and $\Theta = \pi/2$, the upper dashed curves). Here we set $\omega_j/\omega_m = 1$ and choose ω_m as the frequency scale. Other parameters are $G_j/\omega_m = 0.02$, $\gamma_j/\omega_m = 10^{-5}$, $\kappa/\omega_m = 0.2$, and $\bar{n}_j = 100$.

($E_{N,1}$) in the region $0 < \Theta < \pi$ ($\pi < \Theta < 2\pi$). Maximal entanglement emerges at $\Theta = \pi/2$ and $3\pi/2$, which corresponds to the maximal synthetic magnetism. In particular, all the studied types of optomechanical entanglement become much weaker near $\Theta = n\pi$ for an integer n , corresponding to the absence of the synthetic magnetism in the system.

Below, we study how to protect fragile quantum resources from environmental thermal noise by introducing the synthetic magnetism in the nondegenerate-mechanical-mode case. We plot the logarithmic negativity $E_{N,j}$ as functions of the modulation phase Θ and the thermal excitations \bar{n} of the mechanical modes, as shown in Fig. S8. We can see from Figs. S8(a) and S8(b) that, for a given value of \bar{n} , the logarithmic negativities $E_{N,1}$ and $E_{N,2}$ depend on the phase angle Θ . In particular, we have confirmed that, corresponding to a stronger synthetic magnetism, a larger noise tolerance of the quantum entanglement can be obtained [see Figs. S8(a) and S8(b)]. Namely, the maximal synthetic magnetism (i.e., $\Theta = \pi/2$ and $3\pi/2$) leads to the maximal entanglement. These results indicate that, the phase-dependent phonon-hopping interaction (synthetic magnetism) provides a feasible way to protect fragile quantum resources and build noise-tolerant quantum devices. For example, we can see from Fig. S8(c) that the threshold of the quantum entanglement $E_{N,j=1,2}$ can be increased by introducing the phase-dependent phonon-hopping coupling (i.e., the phase in a loop coupling leads to a synthetic magnetism).

3. Entanglement in the blue-detuning regime

In the above subsections, the effect of the synthetic magnetism on the light-vibration entanglement in the red-detuning regime has been studied in detail. Now, we study the dependence of the optomechanical entanglement on the synthetic magnetism in the blue-detuning regime, when the synthetic magnetism is either off or on.

To this end, we plot in Fig. S9 the bipartite entanglement measures $E_{N,j=1,2}$ of the j th vibrational mode with the cavity-field mode as functions of the driving detuning Δ , with and without the synthetic magnetism. We find that when the synthetic magnetism is off, there exists a valley (see lower solid curves) around the blue-sideband resonance (i.e., $\Delta \approx -\omega_m$). However, when turning on the synthetic magnetism, the valley is changed to two peaks around $\Delta \approx -\omega_m$ (see the dashed curves). This means that around the blue-sideband resonance, the light-vibration entanglement is *suppressed* in the absence of the synthetic magnetism. When the synthetic magnetism is present, the light-vibration entanglement is *enhanced* around the blue-sideband resonance. Physically, the introducing synthetic magnetism leads to the breaking of the dark-mode effect, and then it enhances the light-vibration entanglement. Our findings indicate that by introducing the synthetic magnetism, fragile quantum entanglement can be effectively engineered and protected in the blue-detuning regime.

III. DARK MODES AND THEIR BREAKING IN AN OPTOMECHANICAL NETWORK

In this section, we study the dark-mode effect in an optomechanical network, which consists of an optical mode coupled to N ($N \geq 3$) vibrational modes. The nearest-neighboring vibrational modes are coupled to each other through phase-dependent phonon-exchange interactions. For convenience, we here consider the case where there is no interaction between the first

and last mechanical modes. In a rotating frame defined by the transformation operator $\exp(-i\omega_L a^\dagger at)$, the Hamiltonian of the optomechanical network reads

$$H_I = \Delta_c c^\dagger c + \sum_{j=1}^N \omega_j d_j^\dagger d_j + \sum_{j=1}^N g_j c^\dagger c (d_j + d_j^\dagger) + (\Omega c + \Omega^* c^\dagger) + \sum_{j=1}^{N-1} \chi_j (e^{i\Theta_j} d_j^\dagger d_{j+1} + \text{H.c.}), \quad (\text{S50})$$

where $\Delta_c = \omega_c - \omega_L$ is the driving detuning of the cavity-field resonance frequency ω_c with respect to the driving-laser frequency ω_L . The operators c (c^\dagger) and d_j (d_j^\dagger) are, respectively, the annihilation (creation) operators of the cavity-field mode and the j th vibrational mode (with resonance frequency ω_j). The optomechanical interactions between the cavity mode and the j th vibrational mode are described by the g_j terms (with g_j being the single-photon optomechanical-coupling strength). The cavity-field driving is denoted by the Ω term (with Ω being the driving-laser amplitude). To induce synthetic gauge fields in this system, we introduce the phase-dependent phonon-exchange interactions between the nearest-neighbor vibrational modes, with the coupling strength χ_j and the phase Θ_j .

By phenomenologically adding the damping and noise terms into the Heisenberg equations obtained based on the Hamiltonian in Eq. (S50), the quantum Langevin equations for the operators of the optical and mechanical modes are obtained as:

$$\begin{aligned} \dot{c} &= -ic[\Delta_c + \sum_{j=1}^N g_j (d_j + d_j^\dagger)] - i\Omega - \kappa c + \sqrt{2\kappa} c_{\text{in}}, \\ \dot{d}_1 &= -(\gamma_1 + i\omega_1)d_1 - ig_1 c^\dagger c - i\chi_1 e^{i\Theta_1} d_2 + \sqrt{2\gamma_1} d_{1,\text{in}}, \\ \dot{d}_{j \in [2, N-1]} &= -(\gamma_j + i\omega_j)d_j - ig_j c^\dagger c - i\chi_{j-1} e^{-i\Theta_{j-1}} d_{j-1} - i\chi_j e^{i\Theta_j} d_{j+1} + \sqrt{2\gamma_j} d_{j,\text{in}}, \\ \dot{d}_N &= -(\gamma_N + i\omega_N)d_N - ig_N c^\dagger c - i\chi_{N-1} e^{-i\Theta_{N-1}} d_{N-1} + \sqrt{2\gamma_N} d_{N,\text{in}}. \end{aligned} \quad (\text{S51})$$

We also consider the strong-driving regime of the cavity field such that the average photon number in the cavity is sufficiently large. Then the linearization procedure can be used to simplify the physical model. To this end, we express the operators in Eq. (S51) as the sum of their steady-state mean values and quantum fluctuations, namely $o = \langle o \rangle_{\text{ss}} + \delta o$ for operators c , c^\dagger , $d_{j \in [1, N]}$, and d_j^\dagger .

By separating the classical motion of the system from its quantum fluctuations, the classical motion equations take the form as:

$$\begin{aligned} \frac{d}{dt} \langle c \rangle &= - \left\{ \kappa + i \left[\Delta_c + \sum_{j=1}^N g_j (\langle d_j \rangle + \langle d_j^\dagger \rangle) \right] \right\} \langle c \rangle - i\Omega, \\ \frac{d}{dt} \langle d_1 \rangle &= -(\gamma_1 + i\omega_1) \langle d_1 \rangle - ig_1 \langle c^\dagger \rangle \langle c \rangle - i\chi_1 e^{i\Theta_1} \langle d_2 \rangle, \\ \frac{d}{dt} \langle d_{j \in [2, N-1]} \rangle &= -(\gamma_j + i\omega_j) \langle d_j \rangle - ig_j \langle c^\dagger \rangle \langle c \rangle - i\chi_{j-1} e^{-i\Theta_{j-1}} \langle d_{j-1} \rangle - i\chi_j e^{i\Theta_j} \langle d_{j+1} \rangle, \\ \frac{d}{dt} \langle d_N \rangle &= -(\gamma_N + i\omega_N) \langle d_N \rangle - ig_N \langle c^\dagger \rangle \langle c \rangle - i\chi_{N-1} e^{-i\Theta_{N-1}} \langle d_{N-1} \rangle. \end{aligned} \quad (\text{S52})$$

The steady-state mean values of the dynamical variables are obtained as:

$$\begin{aligned} \langle c \rangle_{\text{ss}} &= \frac{-i\Omega}{\kappa + i \left[\Delta_c + \sum_{j=1}^N g_j (\langle d_j \rangle_{\text{ss}} + \langle d_j^\dagger \rangle_{\text{ss}}) \right]}, \\ \langle d_1 \rangle_{\text{ss}} &= \frac{-ig_1 \langle c^\dagger \rangle_{\text{ss}} \langle c \rangle_{\text{ss}} - i\chi_1 e^{i\Theta_1} \langle d_2 \rangle_{\text{ss}}}{\gamma_1 + i\omega_1}, \\ \langle d_{j \in [2, N-1]} \rangle_{\text{ss}} &= \frac{-ig_j \langle c^\dagger \rangle_{\text{ss}} \langle c \rangle_{\text{ss}} - i\chi_{j-1} e^{-i\Theta_{j-1}} \langle d_{j-1} \rangle_{\text{ss}} - i\chi_j e^{i\Theta_j} \langle d_{j+1} \rangle_{\text{ss}}}{\gamma_j + i\omega_j}, \\ \langle d_N \rangle_{\text{ss}} &= \frac{-ig_N \langle c^\dagger \rangle_{\text{ss}} \langle c \rangle_{\text{ss}} - i\chi_{N-1} e^{-i\Theta_{N-1}} \langle d_{N-1} \rangle_{\text{ss}}}{(\gamma_N + i\omega_N)}. \end{aligned} \quad (\text{S53})$$

The linearized equations of motion for the quantum fluctuations are given by:

$$\begin{aligned}
\delta\dot{c} &= -(\kappa + i\Delta)\delta c - i\langle c \rangle_{\text{ss}} \sum_{j=1}^N g_j(\delta d_j + \delta d_j^\dagger) + \sqrt{2\kappa}c_{\text{in}}, \\
\delta\dot{d}_1 &= -(\gamma_1 + i\omega_1)\delta d_1 - ig_1\langle c^\dagger \rangle_{\text{ss}}\delta c - ig_1\langle c \rangle_{\text{ss}}\delta c^\dagger - i\chi_1 e^{i\Theta_1}\delta d_2 + \sqrt{2\gamma_1}d_{1,\text{in}}, \\
\delta\dot{d}_{j \in [2, N-1]} &= -(\gamma_j + i\omega_j)\delta d_j - ig_j\langle c^\dagger \rangle_{\text{ss}}\delta c - ig_j\langle c \rangle_{\text{ss}}\delta c^\dagger - i\chi_{j-1} e^{-i\Theta_{j-1}}\delta d_{j-1} - i\chi_j e^{i\Theta_j}\delta d_{j+1} + \sqrt{2\gamma_j}d_{j,\text{in}}, \\
\delta\dot{d}_N &= -(\gamma_N + i\omega_N)\delta d_N - ig_N\langle c^\dagger \rangle_{\text{ss}}\delta c - ig_N\langle c \rangle_{\text{ss}}\delta c^\dagger - i\chi_{N-1} e^{-i\Theta_{N-1}}\delta d_{N-1} + \sqrt{2\gamma_N}d_{N,\text{in}}.
\end{aligned} \tag{S54}$$

Based on Eqs. (S54), we apply a procedure similar to that used in the two-mechanical-mode case to infer a linearized optomechanical Hamiltonian governing the evolution of the quantum fluctuations. In the N -mechanical-mode case, the linearized optomechanical Hamiltonian takes the form

$$H_I = \Delta\delta c^\dagger\delta c + \omega_j \sum_{j=1}^N \delta d_j^\dagger\delta d_j + \sum_{j=1}^N G_j(\delta c^\dagger\delta d_j + \delta d_j^\dagger\delta c) + H_{\text{mrc}}, \tag{S55}$$

where $\Delta = \Delta_c + \sum_{j=1}^N g_j(\langle d_j \rangle_{\text{ss}} + \langle d_j^\dagger \rangle_{\text{ss}})$ is the normalized driving detuning after the linearization procedure, and $G_j = g_j\langle c \rangle_{\text{ss}}$ is the linearized optomechanical-coupling strength between the j th mechanical mode and the cavity-field mode. The last term in Eq. (S55) is given by

$$H_{\text{mrc}} = \sum_{j=1}^{N-1} H_j, \tag{S56}$$

where the subscript ‘‘mrc’’ stands for the mechanical-resonator coupling of the Hamiltonian, and

$$H_j = \chi_j(e^{-i\Theta_j}\delta d_j\delta d_{j+1}^\dagger + e^{i\Theta_j}\delta d_{j+1}\delta d_j^\dagger), \tag{S57}$$

describes the phonon-exchange interaction between the j th and $(j+1)$ th mechanical modes.

In order to investigate the dark-mode effect in the N -mechanical-mode optomechanical system, we first consider the case where the phase-dependent phonon-exchange interaction is absent, i.e., $H_{\text{mrc}} = 0$. For convenience, we assume that all the mechanical modes have the same resonance frequencies ($\omega_j = \omega_m$) and optomechanical-coupling strengths ($G_j = G$).

In this system, there exists a single bright mode

$$\mathcal{B} = \frac{1}{\sqrt{N}} \sum_{j=1}^N \delta d_j, \tag{S58}$$

and $N-1$ dark modes, which decouple from both the bright mode and the cavity-field mode, with the l th dark mode expressed as

$$\mathcal{D}_{l \in [1, N-1]} = \frac{1}{\sqrt{N}} \sum_{j=1}^N \delta d_j e^{2\pi i(j - \frac{N+1}{2})l/N}. \tag{S59}$$

To break the dark-mode effect in the N -mechanical-mode optomechanical system, we introduce the phase-dependent phonon-exchange interaction H_{mrc} , which, in combination with optomechanical couplings, is used to form a loop-coupled configuration and induce the synthetic magnetism. Without loss of generality, we assume that all the coupling strengths of the phonon-exchange interactions are the same, $\chi_j = \chi$. Thus, we diagonalize the Hamiltonian of these coupled mechanical resonators to get

$$H_{\text{mrt}} = \omega_m \sum_{j=1}^N \delta d_j^\dagger\delta d_j + \chi \sum_{j=1}^{N-1} (e^{-i\Theta_j}\delta d_j\delta d_{j+1}^\dagger + e^{i\Theta_j}\delta d_{j+1}\delta d_j^\dagger) = \sum_{k=1}^N \Omega_k D_k^\dagger D_k, \tag{S60}$$

where the subscript ‘‘mrt’’ stands for the mechanical-resonator terms of the Hamiltonian, and D_k is the k th mechanical normal mode with the resonance frequency

$$\Omega_k = \omega_m + 2\chi \cos\left(\frac{k\pi}{N+1}\right), \quad k = 1, 2, 3, \dots, N. \tag{S61}$$

The mechanical modes δd_j and the normal modes D_k are related by

$$\delta d_j = \begin{cases} \frac{1}{A} \sum_{k=1}^N \sin\left(\frac{k\pi}{N+1}\right) D_k, & j = 1, \\ \frac{1}{A} e^{-i\sum_{v=1}^{j-1} \Theta_v} \sum_{k=1}^N \sin\left(\frac{jk\pi}{N+1}\right) D_k, & j \geq 2, \end{cases} \tag{S62}$$

where we introduce the parameter $A = \sqrt{(N+1)/2}$. The Hamiltonian in Eq. (S55) can be rewritten with these mechanical normal modes as

$$H_I = \Delta \delta c^\dagger \delta c + \sum_{k=1}^N \Omega_k D_k^\dagger D_k + H_{\text{om}}, \quad (\text{S63})$$

where the optomechanical-coupling Hamiltonian H_{om} reads

$$H_{\text{om}} = \sum_{k=1}^N \frac{G}{A} \left[\sin\left(\frac{k\pi}{N+1}\right) + \sum_{j=2}^N e^{i \sum_{v=1}^{j-1} \Theta_v} \sin\left(\frac{jk\pi}{N+1}\right) \right] c D_k^\dagger + \text{H.c.} \quad (\text{S64})$$

It can be seen from Eq. (S64) that the total effect of these phases in the optomechanical interactions is simply determined by the sum $\sum_{v=1}^{j-1} \Theta_v$. Hence, we can apply a single phase to induce the DMB mechanism. For simplicity, we assume $\Theta_j = 0$ for $j = 2, \dots, N-1$ in the following discussions.

As a special case, we first analyze the case of $N = 2$, where the multiple-mechanical-mode optomechanical system is reduced to the two-mechanical-mode optomechanical system, which has been analyzed before. Here, the optomechanical-interaction Hamiltonian Eq. (S64) becomes

$$H_{\text{om}} = \frac{\sqrt{2}G}{2} (1 + e^{i\Theta_1}) c D_1^\dagger + \frac{\sqrt{2}G}{2} (1 - e^{i\Theta_1}) c D_2^\dagger + \text{H.c.} \quad (\text{S65})$$

It is obvious that when $\Theta = n\pi$ for an integer n , the cavity field is decoupled from one of the two hybrid mechanical modes: either D_1 or D_2 . This hybrid mechanical mode, decoupled from the cavity mode, is a dark mode. However, in a general case $\Theta \neq n\pi$, the dark-mode effect is broken, and then the dark-mode-immune optomechanical entanglement becomes accessible under proper parameter conditions.

For the case of $N \geq 3$, the coupling Hamiltonian H_{ck} between the cavity-field mode c and the k th normal mode D_k can be expressed based on Eq. (S64) as

$$H_{\text{ck}} = G_{\text{eff}}^{(k)}(N) c D_k^\dagger + \text{H.c.}, \quad (\text{S66})$$

where the effective coupling coefficient $G_{\text{eff}}^{(k)}(N)$ in Eq. (S66), between the cavity-field mode c and the k th normal mode D_k , can be expressed as

$$G_{\text{eff}}^{(k)}(N) = \frac{G}{A} \left[\sin\left(\frac{k\pi}{N+1}\right) + \sum_{j=2}^N e^{i \sum_{v=1}^{j-1} \Theta_v} \sin\left(\frac{jk\pi}{N+1}\right) \right]. \quad (\text{S67})$$

For convenience, we consider the case of $\Theta_j = 0$ for $j = 2, \dots, (N-1)$, then Eq. (S67) is reduced to

$$G_{\text{eff}}^{(k=\text{odd})}(N = \text{odd}) = \frac{G}{A} \left[(1 + e^{i\Theta_1}) \sin\left(\frac{k\pi}{N+1}\right) + 2e^{i\Theta_1} \sin\left(\frac{2k\pi}{N+1}\right) + 2e^{i\Theta_1} \sin\left(\frac{3k\pi}{N+1}\right) + \dots + 2e^{i\Theta_1} \sin\left(\frac{(N-1)k\pi}{2(N+1)}\right) + e^{i\Theta_1} \sin\left(\frac{k\pi}{2}\right) \right], \quad (\text{S68})$$

$$G_{\text{eff}}^{(k=\text{even})}(N = \text{odd}) = \frac{G}{A} (1 - e^{i\Theta_1}) \sin\left(\frac{k\pi}{N+1}\right), \quad (\text{S69})$$

$$G_{\text{eff}}^{(k=\text{odd})}(N = \text{even}) = \frac{G}{A} \left[(1 + e^{i\Theta_1}) \sin\left(\frac{k\pi}{N+1}\right) + 2e^{i\Theta_1} \sin\left(\frac{2k\pi}{N+1}\right) + 2e^{i\Theta_1} \sin\left(\frac{3k\pi}{N+1}\right) + \dots + 2e^{i\Theta_1} \sin\left(\frac{Nk\pi}{2(N+1)}\right) \right], \quad (\text{S70})$$

$$G_{\text{eff}}^{(k=\text{even})}(N = \text{even}) = G_{\text{eff}}^{(k=\text{even})}(N = \text{odd}). \quad (\text{S71})$$

According to Eqs. (S68)-(S71), we can see that for odd numbers k , the effective coupling strength, between the cavity-field mode c and the k th normal mode D_k , is nonzero, i.e.,

$$G_{\text{eff}}^{(k=\text{odd})}(N) \neq 0. \quad (\text{S72})$$

However, for even numbers k , the coupling strength can be expressed as

$$G_{\text{eff}}^{(k=\text{even})}(N) = \frac{G}{A} (1 - e^{i\Theta_1}) \sin\left(\frac{k\pi}{N+1}\right). \quad (\text{S73})$$

TABLE I: Correspondence of the effective coupling coefficient $G_{\text{eff}}^{(k)}(N)$ [see Eq. (S67)] between the cavity-field mode c and the k th normal mode D_k in various cases when $\Theta_j = 0$ for $j \in \{2, 3, 4, \dots, N-1\}$. We also present the parameter conditions for the dark-mode breaking and the entanglement generation.

	Odd N		Even N		Dark-mode breaking	Entanglement generation [Figs. S10-S11]
	Odd k [Eq. (S73)]	Even k [Eq. (S74)]	Odd k [Eq. (S75)]	Even k [Eq. (S76)]		
$\Theta_1 \neq 2n\pi$	$G_{\text{eff}}^{(k)} \neq 0$	$G_{\text{eff}}^{(k)} \neq 0$	$G_{\text{eff}}^{(k)} \neq 0$	$G_{\text{eff}}^{(k)} \neq 0$	Yes	Yes
$\Theta_1 = 2n\pi$	$G_{\text{eff}}^{(k)} \neq 0$	$G_{\text{eff}}^{(k)} = 0$	$G_{\text{eff}}^{(k)} \neq 0$	$G_{\text{eff}}^{(k)} = 0$	No	No

We can simply see from Eqs. (S66) and (S73) that, when

$$\Theta_1 = 2n\pi, \quad (\text{S74})$$

the effective coupling strength between the even mechanical normal mode $D_{k=\text{even}}$ and the cavity mode c is equal to zero, i.e.,

$$G_{\text{eff}}^{(k=\text{even})}(N) = 0. \quad (\text{S75})$$

In this case, all the even normal modes are decoupled from the cavity field (see Table I). Then optomechanical entanglement cannot be generated in this system due to the dark-mode effect. Thus, these $(N-1)$ dark modes in such optomechanical networks can be broken by tuning the modulation phase (see Table I)

$$\Theta_1 \neq 2n\pi. \quad (\text{S76})$$

This provides the possibility of switching a bosonic-network device between the DMB and DMU regimes.

IV. GENERATION OF QUANTUM ENTANGLEMENT IN OPTOMECHANICAL NETWORKS VIA SYNTHETIC MAGNETISM

In this section, we generalize the DMB mechanism induced by the synthetic magnetism to generate entangled optomechanical networks, which consists of a single cavity field optomechanically coupled to N degenerate vibrational modes.

A. Logarithmic negativity

We introduce the optical and mechanical quadratures and the corresponding Hermitian input noise operators:

$$\begin{aligned} \delta X_o &= (\delta o^\dagger + \delta o) / \sqrt{2}, & \delta Y_o &= i(\delta o^\dagger - \delta o) / \sqrt{2}, \\ X_o^{\text{in}} &= (\delta o_{\text{in}}^\dagger + \delta o_{\text{in}}) / \sqrt{2}, & Y_o^{\text{in}} &= i(\delta o_{\text{in}}^\dagger - \delta o_{\text{in}}) / \sqrt{2}, \end{aligned} \quad (\text{S77})$$

for $o = c, d_1, \dots, d_N$, then the linearized Langevin equations given in (S54) for $N = 5$ can be rewritten as:

$$\begin{aligned}
\delta\dot{X}_c &= -\kappa\delta X_c + \Delta\delta Y_c + \sqrt{2\kappa}X_c^{\text{in}}, \\
\delta\dot{Y}_c &= -\Delta\delta X_c - \kappa\delta Y_c - 2G_1\delta X_{d_1} - 2G_2\delta X_{d_2} - 2G_3\delta X_{d_3} - 2G_4\delta X_{d_4} - 2G_5\delta X_{d_5} + \sqrt{2\kappa}Y_c^{\text{in}}, \\
\delta\dot{X}_{d_1} &= -\gamma_1\delta X_{d_1} + \omega_1\delta Y_{d_1} + \chi_1 \sin \Theta_1 \delta X_{d_2} + \chi_1 \cos \Theta_1 \delta Y_{d_2} + \sqrt{2\gamma_1}X_{d,1}^{\text{in}}, \\
\delta\dot{Y}_{d_1} &= -\omega_1\delta X_{d_1} - \gamma_1\delta Y_{d_1} - 2G_1\delta X_c - \chi_1 \cos \Theta_1 \delta X_{d_2} + \chi_1 \sin \Theta_1 \delta Y_{d_2} + \sqrt{2\gamma_1}Y_{d,1}^{\text{in}}, \\
\delta\dot{X}_{d_2} &= -\gamma_2\delta X_{d_2} + \omega_2\delta Y_{d_2} - \chi_1 \sin \Theta_1 \delta X_{d_1} + \chi_1 \cos \Theta_1 \delta Y_{d_1} + \chi_2 \sin \Theta_2 \delta X_{d_3} + \chi_2 \cos \Theta_2 \delta Y_{d_3} + \sqrt{2\gamma_2}X_{d,2}^{\text{in}}, \\
\delta\dot{Y}_{d_2} &= -\omega_2\delta X_{d_2} - \gamma_2\delta Y_{d_2} - 2G_2\delta X_c - \chi_1 \cos \Theta_1 \delta X_{d_1} - \chi_1 \sin \Theta_1 \delta Y_{d_1} - \chi_2 \cos \Theta_2 \delta X_{d_3} + \chi_2 \sin \Theta_2 \delta Y_{d_3} + \sqrt{2\gamma_2}Y_{d,2}^{\text{in}}, \\
\delta\dot{X}_{d_3} &= -\gamma_3\delta X_{d_3} + \omega_3\delta Y_{d_3} - \chi_2 \sin \Theta_2 \delta X_{d_2} + \chi_2 \cos \Theta_2 \delta Y_{d_2} + \chi_3 \sin \Theta_3 \delta X_{d_4} + \chi_3 \cos \Theta_3 \delta Y_{d_4} + \sqrt{2\gamma_3}X_{d,3}^{\text{in}}, \\
\delta\dot{Y}_{d_3} &= -\omega_3\delta X_{d_3} - \gamma_3\delta Y_{d_3} - 2G_3\delta X_c - \chi_2 \cos \Theta_2 \delta X_{d_2} - \chi_2 \sin \Theta_2 \delta Y_{d_2} - \chi_3 \cos \Theta_3 \delta X_{d_4} + \chi_3 \sin \Theta_3 \delta Y_{d_4} + \sqrt{2\gamma_3}Y_{d,3}^{\text{in}}, \\
\delta\dot{X}_{d_4} &= -\gamma_4\delta X_{d_4} + \omega_4\delta Y_{d_4} - \chi_3 \sin \Theta_3 \delta X_{d_3} + \chi_3 \cos \Theta_3 \delta Y_{d_3} + \chi_4 \sin \Theta_4 \delta X_{d_5} + \chi_4 \cos \Theta_4 \delta Y_{d_5} + \sqrt{2\gamma_4}X_{d,4}^{\text{in}}, \\
\delta\dot{Y}_{d_4} &= -\omega_4\delta X_{d_4} - \gamma_4\delta Y_{d_4} - 2G_4\delta X_c - \chi_3 \cos \Theta_3 \delta X_{d_3} - \chi_3 \sin \Theta_3 \delta Y_{d_3} - \chi_4 \cos \Theta_4 \delta X_{d_5} + \chi_4 \sin \Theta_4 \delta Y_{d_5} + \sqrt{2\gamma_4}Y_{d,4}^{\text{in}}, \\
\delta\dot{X}_{d_5} &= -\gamma_5\delta X_{d_5} + \omega_5\delta Y_{d_5} - \chi_4 \sin \Theta_4 \delta X_{d_4} + \chi_4 \cos \Theta_4 \delta Y_{d_4} + \sqrt{2\gamma_5}X_{d,5}^{\text{in}}, \\
\delta\dot{Y}_{d_5} &= -\omega_5\delta X_{d_5} - \gamma_5\delta Y_{d_5} - 2G_5\delta X_c - \chi_4 \cos \Theta_4 \delta X_{d_4} - \chi_4 \sin \Theta_4 \delta Y_{d_4} + \sqrt{2\gamma_5}Y_{d,5}^{\text{in}}.
\end{aligned} \tag{S78}$$

We proceed to rewrite all the equations in (S78) as the following compact form

$$\dot{\tilde{\mathbf{u}}}(t) = \tilde{\mathbf{A}}\tilde{\mathbf{u}}(t) + \tilde{\mathbf{N}}(t), \tag{S79}$$

where we induce the fluctuation operator vector

$$\tilde{\mathbf{u}}(t) = [\delta X_c, \delta Y_c, \delta X_{d_1}, \delta Y_{d_1}, \delta X_{d_2}, \delta Y_{d_2}, \delta X_{d_3}, \delta Y_{d_3}, \delta X_{d_4}, \delta Y_{d_4}, \delta X_{d_5}, \delta Y_{d_5}]^T, \tag{S80}$$

the noise operator vector

$$\tilde{\mathbf{N}}(t) = \sqrt{2}[\sqrt{\kappa}X_c^{\text{in}}, \sqrt{\kappa}Y_c^{\text{in}}, \sqrt{\gamma_1}X_{d,1}^{\text{in}}, \sqrt{\gamma_1}Y_{d,1}^{\text{in}}, \sqrt{\gamma_2}X_{d,2}^{\text{in}}, \sqrt{\gamma_2}Y_{d,2}^{\text{in}}, \sqrt{\gamma_3}X_{d,3}^{\text{in}}, \sqrt{\gamma_3}Y_{d,3}^{\text{in}}, \sqrt{\gamma_4}X_{d,4}^{\text{in}}, \sqrt{\gamma_4}Y_{d,4}^{\text{in}}, \sqrt{\gamma_5}X_{d,5}^{\text{in}}, \sqrt{\gamma_5}Y_{d,5}^{\text{in}}]^T, \tag{S81}$$

and the coefficient matrix

$$\tilde{\mathbf{A}} = \begin{pmatrix} -\kappa & \Delta & 0 & 0 & 0 & 0 & 0 & 0 & 0 & 0 & 0 & 0 & 0 \\ -\Delta & -\kappa & -2G_1 & 0 & -2G_2 & 0 & -2G_3 & 0 & -2G_4 & 0 & -2G_5 & 0 & 0 \\ 0 & 0 & -\gamma_1 & \omega_1 & \chi_{1+} & \chi_{1-} & 0 & 0 & 0 & 0 & 0 & 0 & 0 \\ -2G_1 & 0 & -\omega_1 & -\gamma_1 & -\chi_{1-} & \chi_{1+} & 0 & 0 & 0 & 0 & 0 & 0 & 0 \\ 0 & 0 & -\chi_{1+} & \chi_{1-} & -\gamma_2 & \omega_2 & \chi_{2+} & \chi_{2-} & 0 & 0 & 0 & 0 & 0 \\ -2G_2 & 0 & -\chi_{1-} & -\chi_{1+} & -\omega_2 & -\gamma_2 & -\chi_{2-} & \chi_{2+} & 0 & 0 & 0 & 0 & 0 \\ 0 & 0 & 0 & 0 & -\chi_{2+} & \chi_{2-} & -\gamma_3 & \omega_3 & \chi_{3+} & \chi_{3-} & 0 & 0 & 0 \\ -2G_3 & 0 & 0 & 0 & -\chi_{2-} & -\chi_{2+} & -\omega_3 & -\gamma_3 & -\chi_{3-} & \chi_{3+} & 0 & 0 & 0 \\ 0 & 0 & 0 & 0 & 0 & 0 & -\chi_{3+} & \chi_{3-} & -\gamma_4 & \omega_4 & \chi_{4+} & \chi_{4-} & 0 \\ -2G_4 & 0 & 0 & 0 & 0 & 0 & -\chi_{3-} & -\chi_{3+} & -\omega_4 & -\gamma_4 & -\chi_{4-} & \chi_{4+} & 0 \\ 0 & 0 & 0 & 0 & 0 & 0 & 0 & 0 & -\chi_{4+} & \chi_{4-} & -\gamma_5 & \omega_5 & 0 \\ -2G_5 & 0 & 0 & 0 & 0 & 0 & 0 & 0 & -\chi_{4-} & -\chi_{4+} & -\omega_5 & -\gamma_5 & 0 \end{pmatrix}, \tag{S82}$$

with $\chi_{j+} = \chi_j \sin \Theta_j$ and $\chi_{j-} = \chi_j \cos \Theta_j$ for $j = 1, \dots, 5$. The formal solution of the linearized Langevin equation (S79) is given by

$$\tilde{\mathbf{u}}(t) = \tilde{\mathbf{M}}(t)\tilde{\mathbf{u}}(0) + \int_0^t \tilde{\mathbf{M}}(t-s)\tilde{\mathbf{N}}(s)ds, \tag{S83}$$

where $\tilde{\mathbf{M}}(t) = \exp(\tilde{\mathbf{A}}t)$. In the following calculations, we set all the parameters to satisfy the stability conditions, which are derived based on the Routh-Hurwitz criterion [S16], i.e., the real parts of all the eigenvalues of $\tilde{\mathbf{A}}$ are negative.

For studying the quantum entanglement between the optical mode and the vibrational modes in the optomechanical networks, we focus on calculating the steady-state value of the covariance matrix $\tilde{\mathbf{V}}$, which is defined by the matrix elements

$$\tilde{V}_{kl} = \frac{1}{2}[\langle \tilde{\mathbf{u}}_k(\infty)\tilde{\mathbf{u}}_l(\infty) \rangle + \langle \tilde{\mathbf{u}}_l(\infty)\tilde{\mathbf{u}}_k(\infty) \rangle], \tag{S84}$$

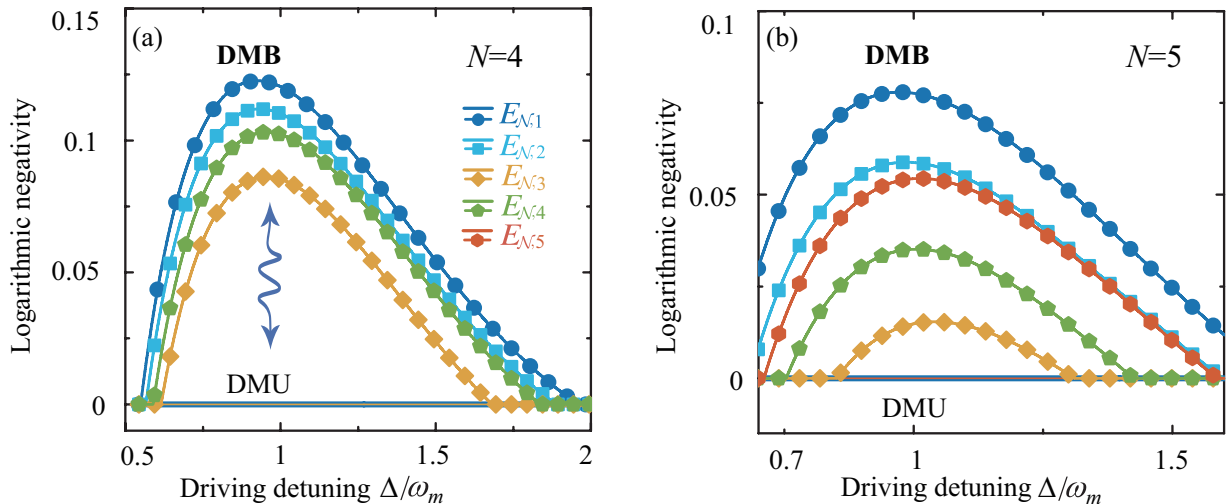


FIG. S10: Optomechanical entanglement $E_{N,j}$ between the cavity-field mode c and the j th mechanical mode d_j versus the effective driving detuning Δ in the DMU ($\chi_j = 0$, solid curves) and DMB ($\chi_j/\omega_m = 0.1$ and $\Theta_1 = \pi$, $\Theta_{j \in [2, N-1]} = 0$, marked by symbols) regimes for (a) $N = 4$ and (b) $N = 5$. Other parameters are the same as those in Fig. S3.

for $k, l = 1, 2, \dots, 12$. Under the stability condition, the covariance matrix $\tilde{\mathbf{V}}$ fulfills the Lyapunov equation

$$\tilde{\mathbf{A}}\tilde{\mathbf{V}} + \tilde{\mathbf{V}}\tilde{\mathbf{A}}^T = -\tilde{\mathbf{Q}}, \quad (\text{S85})$$

where

$$\tilde{\mathbf{Q}} = \text{diag}\{\kappa, \kappa, \gamma_1(2\bar{n}_1 + 1), \gamma_1(2\bar{n}_1 + 1), \gamma_2(2\bar{n}_2 + 1), \gamma_2(2\bar{n}_2 + 1), \dots, \gamma_5(2\bar{n}_5 + 1), \gamma_5(2\bar{n}_5 + 1)\}, \quad (\text{S86})$$

which is defined by

$$\tilde{\mathbf{Q}} = (\tilde{\mathbf{C}} + \tilde{\mathbf{C}}^T)/2, \quad (\text{S87})$$

where $\tilde{\mathbf{C}}$ is the noise correlation matrix, defined by the matrix elements

$$\langle \tilde{\mathbf{N}}_k(s)\tilde{\mathbf{N}}_l(s') \rangle = \tilde{\mathbf{C}}_{k,l}\delta(s - s'). \quad (\text{S88})$$

By using the logarithmic negativity $E_{N,j}$, as shown in Eq. (S34), we can quantify the optomechanical entanglement between the optical mode c and the j th mechanical mode d_j .

B. Optomechanical entanglement networks

We generalize our approach to generate the light-vibration entanglement in an optomechanical-network system, where an optical mode couples to $N \geq 3$ mechanical resonators (MRs) via the optomechanical interactions, and the nearest-neighbour mechanical modes are coupled through the phase-dependent phonon-exchange couplings. We have confirmed that the function of these phases is governed by the term $\sum_{v=1}^{j-1} \Theta_v$ ($j = 2, \dots, N$), and hence, for convenience, we assume $\Theta_1 = \pi$ and $\Theta_{j \in [2, (N-1)]} = 0$ in our simulations.

We demonstrate that, when the synthetic magnetism is absent (i.e., $H_{\text{pec}} = 0$), there only a single bright mode $B_+ = \sum_{j=1}^N \delta d_j / \sqrt{N}$ is induced and $(N-1)$ dark modes are decoupled from the optical mode, and that owing to the synthetic magnetism (the DMB mechanism), all the dark modes can be broken by tuning

In this Section, we study the generation of optomechanical entanglement in the optomechanical networks for the cases of $N = 4$ and 5 . For convenience, we assume that all the mechanical modes have the same resonance frequencies ($\omega_j = \omega_m$ for $j = 1, \dots, N$), the optomechanical-coupling strengths ($G_j = G$ for $j = 1, \dots, N$), and the mechanical-coupling strengths [$\chi_j = \chi$ for $j = 1, \dots, (N-1)$].

To study the dependence of the light-vibration entanglement on the parameters of the system, we show in Figs. S10(a) and S10(b) the optomechanical entanglement measure $E_{N,j}$ of the optical mode with the j th MR as functions of the driving detuning Δ , when the system works in both the DMU and DMB regimes. We reveal that light and all the MRs are separable

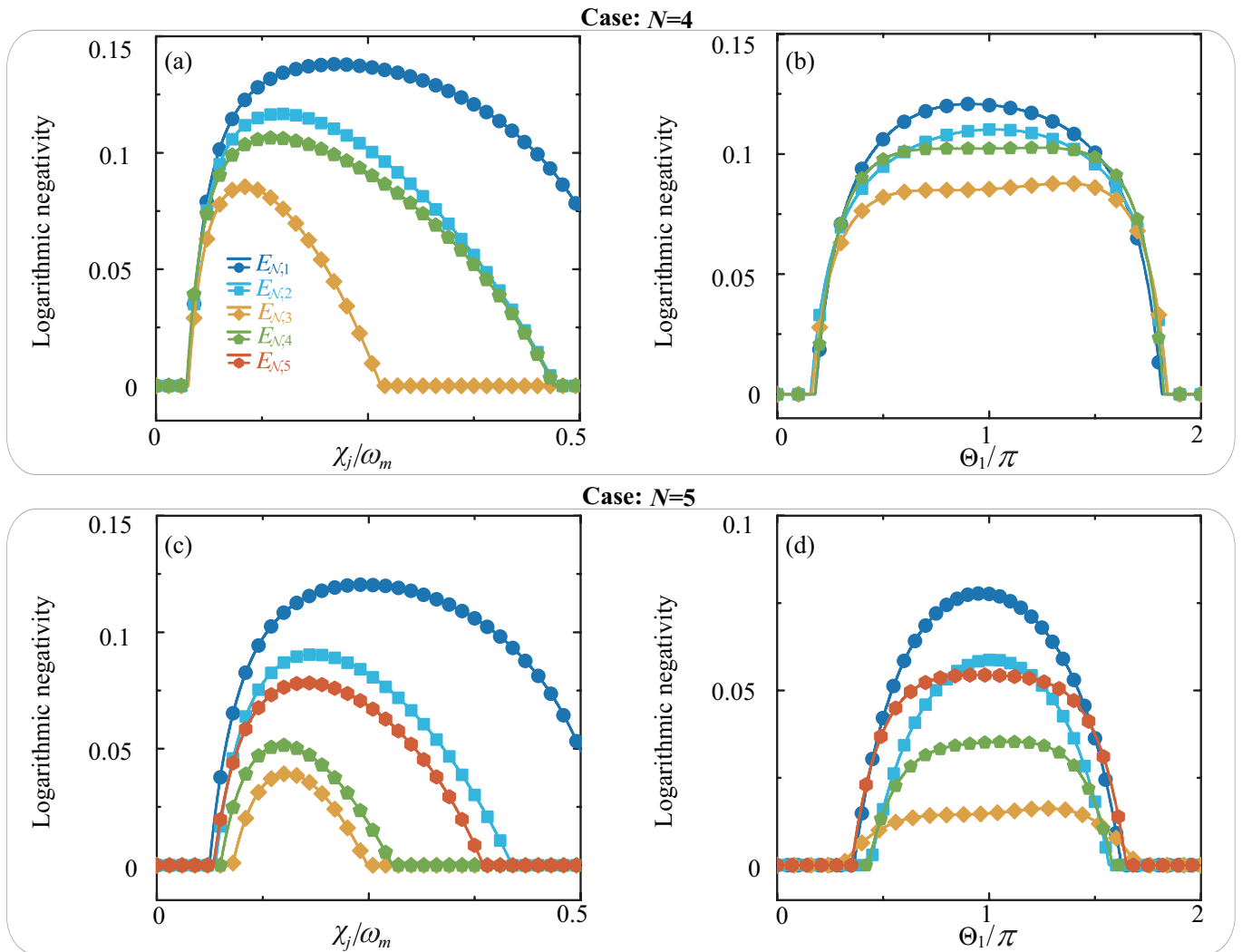


FIG. S11: (a,b) Optomechanical entanglement measure $E_{N,j}$ versus (a) the phonon-hopping coupling strength χ_j when the modulation phase $\Theta_1 = \pi$, and (b) Θ_1 when $\chi_j/\omega_m = 0.1$, for $N = 4$. (c,d) $E_{N,j}$ versus (c) χ_j when $\Theta_1 = \pi$, and (d) Θ_1 when $\chi_j/\omega_m = 0.1$, for $N = 5$. Here we set $\bar{n}_j = 10$, and other parameters are the same as those in Fig. S3.

($E_{N,j} = 0$, see the lower horizontal solid lines) in the DMU regime, but entangled ($E_{N,j} > 0$, see the upper dashed curves) in the DMB regime. This is because in the DMU regime, the thermal excitations concealed in the dark modes cannot be extracted by the optomechanical cooling channel, and it destroys all the quantum entanglement. However, in the DMB regime, quantum entanglement can be achieved around the red-sideband resonance ($\Delta \approx \omega_m$), corresponding to the optimal cooling. Physically, the resulting synthetic magnetism leads to the breaking of all the dark modes, and makes the light-vibration entangled networks feasible. This indicates that dark-mode-immune entangled networks can be realized by applying the DMB mechanism to the optomechanical networks.

Since the synthetic magnetism (DMB mechanism) plays a critical role in the generation of the dark-mode-immune entanglement networks, the dependence of the entanglement networks on the parameters χ and Θ_1 of the synthetic magnetism should be studied in detail. In Fig. S11, we plot the logarithmic negativities $E_{N,j}$ as functions of the mechanical-coupling strength χ and the modulation phase Θ_1 when the system works in the DMB regime. We can see from Figs. S11(a) and S11(c) that the light-vibration entanglement can be generated by tuning the mechanical coupling χ when $\Theta_1 = \pi$, and that the number of the entanglement channels is equal to the number of the mechanical modes. This indicates that the entangled light-vibration networks can be prepared by breaking the dark-mode effect.

In addition, we find from Figs. S11(a) and S11(c) that, in the absence of the synthetic magnetism (i.e., $\chi = 0$), there is no optomechanical entanglement because the system possesses the dark modes and the thermal noise in these dark modes destroys all the quantum correlations. In contrast to this, when we introduce the synthetic magnetism, light and all the vibrational modes become strongly entangled owing to the breaking of the dark modes. Moreover, the maximal optomechanical entanglement can

be observed for $\chi \approx 0.15\omega_m$ when $\Theta_1 = \pi$. Physically, the application of the synthetic magnetism provides the physical origin for breaking the dark-mode effect and generating optomechanical entanglement. These results show a clear perspective for creating quantum resources against the dark-mode effect.

Moreover, we find from Figs. S11(b) and S11(d) that the optomechanical entanglement is generated in the region $0 < \Theta_1 < 2\pi$, and that the maximal entanglement emerges around $\Theta_1 \approx \pi$. Additionally, light and all the vibrations are disentangled (i.e., $E_{N,j} = 0$) around $\Theta_1 \approx 2n\pi$ for an integer n , which corresponds to the emergence of the dark-mode effect. Hence it is possible to flexibly switch the dark-mode immune entanglement on and off on demand by tuning the modulation phase Θ_1 . These results indicate that dark-mode-immune entangled optomechanical networks can be realized by using the DMB mechanism to optomechanical networks. Our findings enable constructing large-scale entangled networks and switches with dark-mode immunity and noise tolerance, and open up a range of exciting opportunities for quantum information processing and quantum metrology with tolerance against the dark modes.

V. DISCUSSIONS ON THE EXPERIMENTAL REALIZATIONS OF OUR PHYSICAL MODEL

The proposed physical model is general and hence it can be implemented using optomechanical platforms in which the involved interactions can be realized. To generate both the dark-mode-immune and noise-tolerant entanglement, our model relies on two kinds of interactions: one is the in-parallel optomechanical interactions between the optical mode and multiple vibrational modes, and the other type is a phase-dependent phonon-hopping interaction (i.e., the phase in a loop coupling leads to an effective synthetic magnetism) between a pair of nearest-neighbor vibrational modes. Therefore, the two kinds of interactions could be implemented in our candidate experimental systems. It should be pointed out that, though until now the two kinds of couplings have been realized in separate experiments, the implementation of these two kinds of couplings in the same experimental setup has not been reported yet. Nevertheless, we are positive that the two kinds of interactions can be implemented in our system under current or near-future experimental conditions. Note that experimental capabilities in this field have improved enormously over the past decade and will continue to improve enormously over the next decade, allowing vastly improved experimental possibilities.

Currently, the in-parallel optomechanical couplings have been experimentally implemented in both optical [S23–S25] and microwave [S2, S5, S26–S29] domains. In the optical domain, the in-parallel optomechanical couplings can be experimentally implemented using either the “membrane-in-the-middle” optomechanical systems [S23, S24] or the multi-membrane Fabry-Pérot-cavity optomechanical configurations [S25]. In the microwave domain, one can use a microwave-frequency realization of cavity optomechanical systems involving multiple micromechanical drum oscillators and a superconducting on-chip circuit acting as an electromagnetic cavity [S2, S5, S26–S29]. The vibration of the mechanical resonators affect the total capacitance and thus modulate the frequency of the cavity. This creates the in-parallel optomechanical interactions similar to those between a cavity mode and multiple resonators in an optical cavity [S2, S5, S26–S29].

The phase-dependent phonon-hopping coupling between the nearest-neighbor mechanical resonators could be implemented by using either photonic-crystal optomechanical-cavity systems [S10] or circuit electromechanical systems [S2, S5, S26–S29]. In the photonic-crystal optomechanical-cavity setup, this phonon-hopping coupling can be induced by using two auxiliary cavity fields (see Sec. V A). In the circuit electromechanical system, this phonon-hopping coupling can be indirectly induced by coupling the two mechanical resonators to a superconducting charge qubit (see Sec. V B).

Based on the above-mentioned experimental advances in both the in-parallel optomechanical couplings and phase-dependent phonon-hopping interactions, we propose to implement our physical model using either a photonic-crystal optomechanical-cavity system [S10] (as shown in Fig. S12) or a circuit electromechanical system (as shown in Fig. S15). Below, we present detailed discussions on the experimental implementations of our scheme in the above-mentioned two setups. In particular, we present some parameter analyses and numerical simulations to demonstrate that the proposed phenomena are relevant for the state-of-the-art experiments based on these two platforms.

A. Experimental realization of the proposed model based on the photonic-crystal optomechanical system

Recently, the synthetic magnetism has been reported in a photonic-crystal optomechanical-cavity setup with both optical and mechanical couplings between two optomechanical cavities [S10]. Motivated by this experimental advance, we propose to implement our physical model using this photonic-crystal optomechanical system. Specifically, we present a detailed derivation of an effective Hamiltonian from the original Hamiltonian based on the photonic-crystal optomechanical-cavity platform. Note that the validity of the effective Hamiltonian has been confirmed by checking the consistence of the induced physical effects.

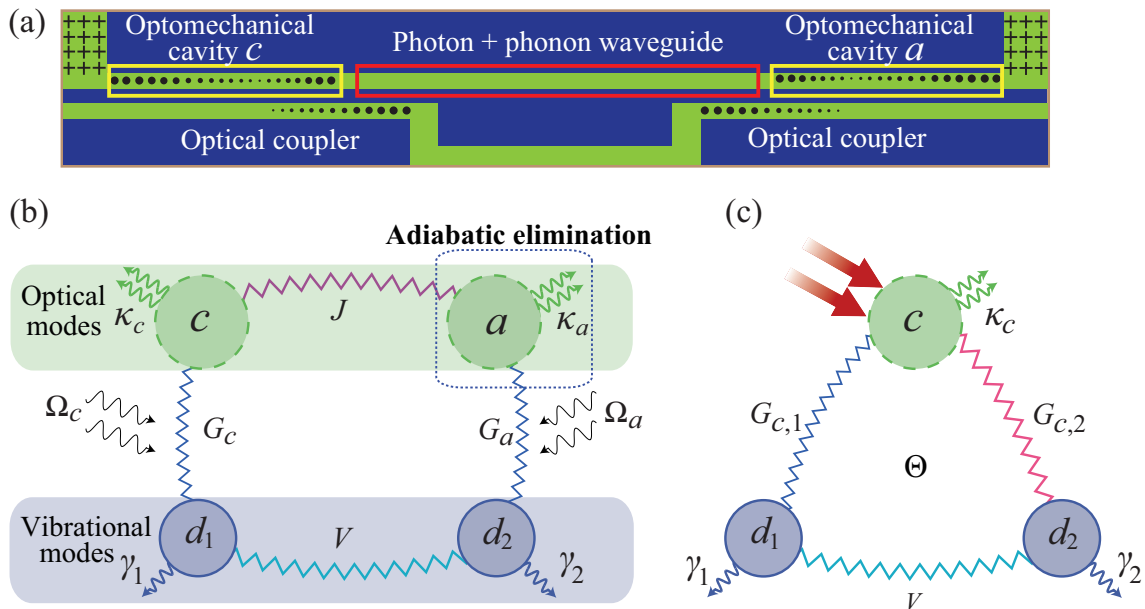


FIG. S12: (a) A proposed implementation of our model and the effective synthetic magnetic field based on a photonic-crystal optomechanical circuit, which could be fabricated from a silicon-on-insulator microchip, consisting of left and right nanobeam optomechanical-crystal cavities with a central unpatterned nanobeam waveguide connecting two optomechanical cavities. The left and right optical couplers are each fed by an adiabatic fiber-to-chip coupler, and they are used for evanescently coupling light into either of the two optical cavities. (b) This optomechanical circuit can be reduced to a four-mode optomechanical system, where the two optical modes (c and a) are coupled to each other through a photon-hopping coupling J , and the two vibrational modes (d_1 and d_2) are coupled to each other via a phonon-hopping at a rate V , with J and V set to be real for an appropriate choice of gauge. (c) By adiabatically eliminating the auxiliary cavity-field mode a in the large-detuning regime, the model in (b) can be reduced to a three-mode loop-coupled optomechanical system consisting of two coupled mechanical modes (d_1 and d_2) coupled to a single cavity-field mode (c). Pumping of the optomechanical cavities with phase-correlated lasers results in an effective synthetic magnetic field.

1. Detailed derivation of the effective Hamiltonian H_{eff}

Based on a four-mode photonic-crystal optomechanical-cavity system, our physical model can be effectively derived by adiabatically eliminating a single cavity-field mode in the large-detuning regime. Thus, we first consider an original physical system, where both the optical and mechanical interactions are induced between the two optomechanical cavities [see Fig. S12(a)], and the Hamiltonian of the system reads

$$H = \omega_c c^\dagger c + \omega_a a^\dagger a + \omega_1 d_1^\dagger d_1 + \omega_2 d_2^\dagger d_2 + g_c c^\dagger c (d_1^\dagger + d_1) + g_a a^\dagger a (d_2^\dagger + d_2) + J(c^\dagger a + a^\dagger c) + V(d_1^\dagger d_2 + d_2^\dagger d_1) + (\Omega_c c e^{i\omega_{L,c}t} + \Omega_c^* c^\dagger e^{-i\omega_{L,c}t}) + (\Omega_a a e^{i\omega_{L,a}t} + \Omega_a^* a^\dagger e^{-i\omega_{L,a}t}), \quad (\text{S89})$$

where c^\dagger (c), a^\dagger (a), and d_j^\dagger (d_j) are the creation (annihilation) operators of the two optical modes (with resonance frequencies ω_c and ω_a) and the j th vibrational mode (with resonance frequency ω_j), respectively. The g_c and g_a terms describe optomechanical interactions between the cavity-field mode and the vibrational modes, with g_c and g_a being the single-photon optomechanical-coupling strengths. The J and V terms are, respectively, the photon-hopping and phonon-hopping interactions, while the Ω_c and Ω_a terms describe the cavity-field drivings for the two cavities.

In the rotating frame defined by the unitary transformation operator $\exp[-i(\omega_{L,a} a^\dagger a + \omega_{L,c} c^\dagger c)t]$ under $\omega_{L,a} = \omega_{L,c}$, the Hamiltonian in Eq. (S89) becomes

$$H_I = \Delta_c c^\dagger c + \Delta_a a^\dagger a + \omega_1 d_1^\dagger d_1 + \omega_2 d_2^\dagger d_2 + g_{c,1} c^\dagger c (d_1^\dagger + d_1) + g_a a^\dagger a (d_2^\dagger + d_2) + J(c^\dagger a + a^\dagger c) + V(d_1^\dagger d_2 + d_2^\dagger d_1) + (\Omega_c c + \Omega_c^* c^\dagger) + (\Omega_a a + \Omega_a^* a^\dagger), \quad (\text{S90})$$

where $\Delta_{k=a,c} = \omega_k - \omega_{L,k}$ denotes the cavity-field driving detuning of the k th cavity. By phenomenologically adding the damping and noise terms into the Heisenberg equations, obtained using the Hamiltonian in Eq. (S90), we obtain the quantum Langevin

equations for the operators of the optical and mechanical modes:

$$\begin{aligned}
\dot{c} &= -i\Delta_c c - ig_c c (d_1^\dagger + d_1) - iJ a - i\Omega_c^* - \kappa_c c + \sqrt{2\kappa_c} c_{\text{in}}, \\
\dot{a} &= -i\Delta_a a - ig_a a (d_2^\dagger + d_2) - iJ c - i\Omega_a^* - \kappa_a a + \sqrt{2\kappa_a} a_{\text{in}}, \\
\dot{d}_1 &= -i\omega_1 d_1 - ig_c c^\dagger c - iV d_2 - \gamma_1 d_1 + \sqrt{2\gamma_1} d_{1,\text{in}}, \\
\dot{d}_2 &= -i\omega_2 d_2 - ig_a a^\dagger a - iV d_1 - \gamma_2 d_2 + \sqrt{2\gamma_2} d_{2,\text{in}},
\end{aligned} \tag{S91}$$

where the operators c_{in} and $d_{j=1,2,\text{in}}$ are introduced in Eq. S3, and operator a_{in} is input noise operator for the optical mode a . We consider the strong-driving regime of the cavity fields, then the average photon number in the cavities can be sufficiently large. In this case, we can use the linearization procedure to simplify the physical model. To this end, we express the operators in Eq. (S91) as the sum of their steady-state mean values and quantum fluctuations, namely $o = \langle o \rangle_{\text{ss}} + \delta o$ for operators $o = a, a^\dagger, c, c^\dagger, d_{j=1,2}$, and $d_{j=1,2}^\dagger$. We can separate the classical motions from the quantum fluctuations, and then the equations take the form as:

$$\begin{aligned}
\frac{d}{dt} \langle c \rangle &= -(\kappa_c + i\Delta'_c) \langle c \rangle - iJ \langle a \rangle - i\Omega_c^*, \\
\frac{d}{dt} \langle a \rangle &= -(\kappa_a + i\Delta'_a) \langle a \rangle - iJ \langle c \rangle - i\Omega_a^*, \\
\frac{d}{dt} \langle d_1 \rangle &= -(\gamma_1 + i\omega_1) \langle d_1 \rangle - ig_c \langle c^\dagger \rangle \langle c \rangle - iV \langle d_2 \rangle, \\
\frac{d}{dt} \langle d_2 \rangle &= -(\gamma_2 + i\omega_2) \langle d_2 \rangle - ig_a \langle a^\dagger \rangle \langle a \rangle - iV \langle d_1 \rangle.
\end{aligned} \tag{S92}$$

Based on Eq. (S92), the steady-state mean values of the dynamical variables are:

$$\begin{aligned}
\langle c \rangle_{\text{ss}} &= \frac{iJ \langle a \rangle_{\text{ss}} + i\Omega_c^*}{-(\kappa_c + i\Delta'_c)}, & \langle a \rangle_{\text{ss}} &= \frac{iJ \langle c \rangle_{\text{ss}} + i\Omega_a^*}{-(\kappa_a + i\Delta'_a)}, \\
\langle d_1 \rangle_{\text{ss}} &= \frac{ig_c \langle c^\dagger \rangle_{\text{ss}} \langle c \rangle_{\text{ss}} + iV \langle d_2 \rangle_{\text{ss}}}{-(\gamma_1 + i\omega_1)}, & \langle d_2 \rangle_{\text{ss}} &= \frac{ig_a \langle a^\dagger \rangle_{\text{ss}} \langle a \rangle_{\text{ss}} + iV \langle d_1 \rangle_{\text{ss}}}{-(\gamma_2 + i\omega_2)},
\end{aligned} \tag{S93}$$

where we introduce the effective driving detuning of the two cavity fields $\Delta'_c = \Delta_c + g_c(\langle d_1^\dagger \rangle + \langle d_1 \rangle)$ and $\Delta'_a = \Delta_a + g_a(\langle d_2^\dagger \rangle + \langle d_2 \rangle)$. The linearized equations of motion for the quantum fluctuations are given by:

$$\begin{aligned}
\delta \dot{c} &= -(\kappa_c + i\Delta'_c) \delta c - iG_c (\delta d_1^\dagger + \delta d_1) - iJ \delta a + \sqrt{2\kappa_c} c_{\text{in}}, \\
\delta \dot{a} &= -(\kappa_a + i\Delta'_a) \delta a - iG_a (\delta d_2^\dagger + \delta d_2) - iJ \delta c + \sqrt{2\kappa_a} a_{\text{in}}, \\
\delta \dot{d}_1 &= -(\gamma_1 + i\omega_1) \delta d_1 - iG_c \delta c^\dagger - iG_c^* \delta c - iV \delta d_2 + \sqrt{2\gamma_1} d_{1,\text{in}}, \\
\delta \dot{d}_2 &= -(\gamma_2 + i\omega_2) \delta d_2 - iG_a \delta a^\dagger - iG_a^* \delta a - iV \delta d_1 + \sqrt{2\gamma_2} d_{2,\text{in}},
\end{aligned} \tag{S94}$$

where the effective optomechanical-coupling strengths between the first (second) mechanical resonator and the cavity-field mode c (a) are, respectively, defined as: $G_c = g_c \langle c \rangle$ and $G_a = g_a \langle a \rangle$. Based on Eq. (S94), we obtain the linearized Hamiltonian

$$\begin{aligned}
H_{\text{lin}} &= \Delta'_c \delta c^\dagger \delta c + \Delta'_a \delta a^\dagger \delta a + \omega_1 \delta d_1^\dagger \delta d_1 + \omega_2 \delta d_2^\dagger \delta d_2 + J(\delta c^\dagger \delta a + \delta a^\dagger \delta c) + V(\delta d_1^\dagger \delta d_2 + \delta d_2^\dagger \delta d_1) \\
&+ (G_{c,1} \delta c^\dagger + G_{c,1}^* \delta c)(\delta d_1^\dagger + \delta d_1) + (G_a \delta a^\dagger + G_a^* \delta a)(\delta d_2^\dagger + \delta d_2).
\end{aligned} \tag{S95}$$

In the rotating frame with respect to $H_0 = \Delta'_c \delta c^\dagger \delta c + \Delta'_a \delta a^\dagger \delta a + \omega_1 \delta d_1^\dagger \delta d_1 + \omega_2 \delta d_2^\dagger \delta d_2$, the Hamiltonian becomes

$$\begin{aligned}
H'_1 &= J[\delta c^\dagger \delta a e^{i(\Delta'_c - \Delta'_a)t} + \delta a^\dagger \delta c e^{i(\Delta'_a - \Delta'_c)t}] + V[\delta d_1^\dagger \delta d_2 e^{i(\omega_1 - \omega_2)t} + \delta d_2^\dagger \delta d_1 e^{i(\omega_2 - \omega_1)t}] \\
&+ G_c \delta c^\dagger \delta d_1^\dagger e^{i(\Delta'_c + \omega_1)t} + G_c \delta c^\dagger \delta d_1 e^{i(\Delta'_c - \omega_1)t} + G_c^* \delta c \delta d_1^\dagger e^{-i(\Delta'_c - \omega_1)t} \\
&+ G_c^* \delta c \delta d_1 e^{-i(\Delta'_c + \omega_1)t} + G_a \delta a^\dagger \delta d_2^\dagger e^{i(\Delta'_a + \omega_2)t} + G_a \delta a^\dagger \delta d_2 e^{i(\Delta'_a - \omega_2)t} \\
&+ G_a^* \delta a \delta d_2^\dagger e^{-i(\Delta'_a - \omega_2)t} + G_a^* \delta a \delta d_2 e^{-i(\Delta'_a + \omega_2)t}.
\end{aligned} \tag{S96}$$

To obtain the effective Hamiltonian describing our physical model, we consider the case of $\Delta'_c = \omega_{j=1,2}$, and then the Hamiltonian in Eq. (S96) can be expressed as

$$H'_1 = H'_0 + \sum_{n=1}^3 (h_n e^{-i\tilde{\omega}_n t} + h.c.), \tag{S97}$$

where

$$H'_0 = V(\delta d_1^\dagger \delta d_2 + \delta a_2^\dagger \delta d_1) + (G_c \delta c^\dagger \delta d_1 + G_c^* \delta c \delta d_1^\dagger), \quad (\text{S98})$$

and

$$\begin{aligned} h_1 &= J \delta c^\dagger \delta a + G_a^* \delta a \delta d_2^\dagger, & h_2 &= G_c^* \delta c \delta d_1, & h_3 &= G_a^* \delta a \delta d_2, \\ \tilde{\omega}_1 &= \Delta'_a - \omega_2, & \tilde{\omega}_2 &= \Delta'_c + \omega_1, & \tilde{\omega}_3 &= \Delta'_a + \omega_2. \end{aligned} \quad (\text{S99})$$

In the large-detuning regime of the cavity-field mode a , we can adiabatically eliminate the cavity mode a and then obtain the effective Hamiltonian [S33]

$$\begin{aligned} H'_{\text{eff}} &= H'_0 + \sum_{n,m}^3 \frac{1}{\tilde{\omega}_{n,m}^+} [h_m^\dagger, h_n] e^{i(\tilde{\omega}_m - \tilde{\omega}_n)t} \\ &= H'_0 + \frac{1}{\tilde{\omega}_{1,1}^+} [h_1^\dagger, h_1] e^{i(\tilde{\omega}_1 - \tilde{\omega}_1)t} + \frac{1}{\tilde{\omega}_{2,1}^+} [h_1^\dagger, h_2] e^{i(\tilde{\omega}_1 - \tilde{\omega}_2)t} + \frac{1}{\tilde{\omega}_{3,1}^+} [h_1^\dagger, h_3] e^{i(\tilde{\omega}_1 - \tilde{\omega}_3)t} \\ &\quad + \frac{1}{\tilde{\omega}_{1,2}^+} [h_2^\dagger, h_1] e^{i(\tilde{\omega}_2 - \tilde{\omega}_1)t} + \frac{1}{\tilde{\omega}_{2,2}^+} [h_2^\dagger, h_2] e^{i(\tilde{\omega}_2 - \tilde{\omega}_2)t} + \frac{1}{\tilde{\omega}_{3,2}^+} [h_2^\dagger, h_3] e^{i(\tilde{\omega}_2 - \tilde{\omega}_3)t} \\ &\quad + \frac{1}{\tilde{\omega}_{1,3}^+} [h_3^\dagger, h_1] e^{i(\tilde{\omega}_3 - \tilde{\omega}_1)t} + \frac{1}{\tilde{\omega}_{2,3}^+} [h_3^\dagger, h_2] e^{i(\tilde{\omega}_3 - \tilde{\omega}_2)t} + \frac{1}{\tilde{\omega}_{3,3}^+} [h_3^\dagger, h_3] e^{i(\tilde{\omega}_3 - \tilde{\omega}_3)t}, \end{aligned} \quad (\text{S100})$$

By considering the resonance case (i.e., $n = m$), and dropping high-frequency components, the Hamiltonian in Eq. (S100) becomes

$$H'_{\text{eff}} \approx H'_0 + \frac{1}{\tilde{\omega}_{1,1}^+} [h_1^\dagger, h_1] + \frac{1}{\tilde{\omega}_{2,2}^+} [h_2^\dagger, h_2] + \frac{1}{\tilde{\omega}_{3,3}^+} [h_3^\dagger, h_3], \quad (\text{S101})$$

where

$$\frac{1}{\tilde{\omega}_{n,m}^+} = \frac{1}{2} \left(\frac{1}{\tilde{\omega}_n} + \frac{1}{\tilde{\omega}_m} \right). \quad (\text{S102})$$

By pumping the optomechanical cavities with phase-correlated lasers, the linearized optomechanical-coupling strengths, with the modulation phases, can be defined as

$$\begin{aligned} G_c &= G_{c,1} e^{i\Theta_1}, \quad \text{for } G_{c,1} = g_c |\langle c \rangle_{\text{ss}}|, \\ G_a &= g_a |\langle a \rangle_{\text{ss}}| e^{i\Theta_2}. \end{aligned} \quad (\text{S103})$$

We consider the case of $\Theta_1 = \Theta$ and $\Theta_2 = 0$, then the effective Hamiltonian given in Eq. (S101) becomes

$$\begin{aligned} H'_{\text{eff}} &\approx \delta \omega_c \delta c^\dagger \delta c + \delta \omega_1 \delta a_1^\dagger \delta d_1 + \delta \omega_2 \delta a_2^\dagger \delta d_2 + V(\delta a_1^\dagger \delta d_2 + \delta d_1^\dagger \delta a_1) \\ &\quad + (G_{c,1} e^{i\Theta} \delta c^\dagger \delta d_1 + G_{c,1} e^{-i\Theta} \delta c \delta d_1^\dagger) + (G_{c,2} \delta c^\dagger \delta d_2 + G_{c,2}^* \delta c \delta d_2^\dagger), \end{aligned} \quad (\text{S104})$$

where $\delta \omega_c = -|G_c|^2 / (\Delta'_c + \omega_1) - J^2 / (\Delta'_a - \omega_2)$, $\delta \omega_1 = -|G_c|^2 / (\Delta'_c + \omega_1)$, $\delta \omega_2 = -2|G_a|^2 \Delta'_a / (\Delta_a'^2 - \omega_2^2)$, and $G_{c,2} = JG_a / (\omega_2 - \Delta'_a)$. By introducing a rotating operator $R(\Theta) = e^{i\Theta d_1^\dagger}$, the effective Hamiltonian present in Eq. (S104) becomes

$$\begin{aligned} H'_{\text{eff}} &\approx \delta \omega_c \delta c^\dagger \delta c + \delta \omega_1 \delta d_1^\dagger \delta d_1 + \delta \omega_2 \delta d_2^\dagger \delta d_2 + V(e^{i\Theta} \delta d_1^\dagger \delta d_2 + e^{-i\Theta} \delta d_2^\dagger \delta d_1) \\ &\quad + (G_{c,1} \delta c^\dagger \delta d_1 + G_{c,1} \delta c \delta d_1^\dagger) + (G_{c,2} \delta c^\dagger \delta d_2 + G_{c,2}^* \delta c \delta d_2^\dagger). \end{aligned} \quad (\text{S105})$$

In the original frame, it is seen that H'_{eff} is transformed to

$$\begin{aligned} H_{\text{eff}} &\approx \tilde{\Delta}'_c \delta c^\dagger \delta c + \omega'_1 \delta d_1^\dagger \delta d_1 + \omega'_2 \delta d_2^\dagger \delta d_2 + V(e^{i\Theta} \delta d_1^\dagger \delta d_2 + e^{-i\Theta} \delta d_2^\dagger \delta d_1) \\ &\quad + (G_{c,1} \delta c^\dagger \delta d_1 + G_{c,1} \delta c \delta d_1^\dagger) + (G_{c,2} \delta c^\dagger \delta d_2 + G_{c,2}^* \delta c \delta d_2^\dagger), \end{aligned} \quad (\text{S106})$$

where the effective driving detuning of the cavity mode c and the effective mechanical frequency of the j th mechanical resonator are defined, respectively, as $\tilde{\Delta}'_c = \Delta'_c + \delta \omega_c$ and $\omega'_j = \omega_j + \delta \omega_j$. It is shown in Eq. (S106) that the proposed scheme and the synthetic magnetism can be effectively realized by using current experimental conditions in the photonic-crystal optomechanical-cavity systems, as shown in Fig. S12.

2. Optomechanical entanglement in the photonic-crystal optomechanical system

In this section, we calculate optomechanical entanglement in the photonic-crystal optomechanical-cavity system (with it making the approximations). We also compare these entanglement results with the supposed results (i.e., the entanglement discussed in our three-mode case). The motivation for this comparison is to confirm that our supposed results can be obtained in the photonic-crystal optomechanical setup. Specifically, we derive the steady-state variance matrix and adopt the logarithmic negativity to quantify the optomechanical entanglement in the photonic-crystal optomechanical system. For the present system, the linearized Langevin equations given in (S94) can be rewritten with the quadrature operators as:

$$\begin{aligned}
\delta\dot{X}_c &= -\kappa_c\delta X_c + \Delta'_c\delta Y_c + J\delta Y_a + i(G_c^* - G_c)\delta X_{d_1} + \sqrt{2\kappa_c}X_c^{\text{in}}, \\
\delta\dot{Y}_c &= -\Delta'_c\delta X_c - \kappa_c\delta Y_c - J\delta X_a - (G_c + G_c^*)\delta X_{d_1} + \sqrt{2\kappa_c}Y_c^{\text{in}}, \\
\delta\dot{X}_a &= -\kappa_a\delta X_a + \Delta'_a\delta Y_a + J\delta Y_c + i(G_a^* - G_a)\delta X_{d_2} + \sqrt{2\kappa_a}X_a^{\text{in}}, \\
\delta\dot{Y}_a &= -\Delta'_a\delta X_a - \kappa_a\delta Y_a - J\delta X_c - (G_a^* + G_a)\delta X_{d_2} + \sqrt{2\kappa_a}Y_a^{\text{in}}, \\
\delta\dot{X}_{d_1} &= -\gamma_1\delta X_{d_1} + \omega_1\delta Y_{d_1} + V\delta Y_{d_2} + \sqrt{2\gamma_1}X_{d,1}^{\text{in}}, \\
\delta\dot{Y}_{d_1} &= -(G_c + G_c^*)\delta X_c - i(G_c^* - G_c)\delta Y_c - \omega_1\delta X_{d_1} - \gamma_1\delta Y_{d_1} - V\delta X_{d_2} + \sqrt{2\gamma_1}Y_{d,1}^{\text{in}}, \\
\delta\dot{X}_{d_2} &= -\gamma_2\delta X_{d_2} + \omega_2\delta Y_{d_2} + V\delta Y_{d_1} + \sqrt{2\gamma_2}X_{d,2}^{\text{in}}, \\
\delta\dot{Y}_{d_2} &= -G_a^*(\delta X_a + i\delta Y_a) - G_a(\delta X_a - i\delta Y_a) - V\delta X_{d_1} - \omega_2\delta X_{d_2} - \gamma_2\delta Y_{d_2} + \sqrt{2\gamma_2}Y_{d,2}^{\text{in}},
\end{aligned} \tag{S107}$$

We proceed to rewrite equations in (S107) as the following compact form

$$\dot{\tilde{\mathbf{u}}}(t) = \tilde{\mathbf{A}}\tilde{\mathbf{u}}(t) + \tilde{\mathbf{N}}(t), \tag{S108}$$

where we induce the fluctuation operator vector

$$\tilde{\mathbf{u}}(t) = [\delta X_c, \delta Y_c, \delta X_a, \delta Y_a, \delta X_{d_1}, \delta Y_{d_1}, \delta X_{d_2}, \delta Y_{d_2}]^T, \tag{S109}$$

the noise operator vector

$$\tilde{\mathbf{N}}(t) = \sqrt{2}[\sqrt{\kappa_c}X_c^{\text{in}}, \sqrt{\kappa_c}Y_c^{\text{in}}, \sqrt{\kappa_a}X_a^{\text{in}}, \sqrt{\kappa_a}Y_a^{\text{in}}, \sqrt{\gamma_1}X_{d,1}^{\text{in}}, \sqrt{\gamma_1}Y_{d,1}^{\text{in}}, \sqrt{\gamma_2}X_{d,2}^{\text{in}}, \sqrt{\gamma_2}Y_{d,2}^{\text{in}}]^T, \tag{S110}$$

and the coefficient matrix

$$\tilde{\mathbf{A}} = \begin{pmatrix} -\kappa_c & +\Delta'_c & 0 & J & i(G_c^* - G_c) & 0 & 0 & 0 \\ -\Delta'_c & -\kappa_c & -J & 0 & -(G_c^* + G_c) & 0 & 0 & 0 \\ 0 & J & -\kappa_a & \Delta'_a & 0 & 0 & i(G_a^* - G_a) & 0 \\ -J & 0 & -\Delta'_a & -\kappa_a & 0 & 0 & -(G_a^* + G_a) & 0 \\ 0 & 0 & 0 & 0 & -\gamma_1 & \omega_1 & 0 & V \\ -(G_c^* + G_c) & -i(G_c^* - G_c) & 0 & 0 & -\omega_1 & -\gamma_1 & -V & 0 \\ 0 & 0 & 0 & 0 & 0 & 0 & -\gamma_2 & \omega_2 \\ 0 & 0 & -(G_a^* + G_a) & -i(G_a^* - G_a) & -V & 0 & -\omega_2 & -\gamma_2 \end{pmatrix}. \tag{S111}$$

The formal solution of the linearized Langevin equation (S108) is given by

$$\tilde{\mathbf{u}}(t) = \tilde{\mathbf{M}}(t)\tilde{\mathbf{u}}(0) + \int_0^t \tilde{\mathbf{M}}(t-s)\tilde{\mathbf{N}}(s)ds, \tag{S112}$$

where $\tilde{\mathbf{M}}(t) = \exp(\tilde{\mathbf{A}}t)$. In the following calculations, we set all the parameters to satisfy the stability conditions derived using the Routh-Hurwitz criterion [S16]. This means that the real parts of all the eigenvalues of $\tilde{\mathbf{A}}$ are negative.

For studying the quantum entanglement between the optical mode and the vibrational modes in the photonic-crystal optomechanical-cavity system, we focus on calculating the steady-state value of the covariance matrix $\tilde{\mathbf{V}}$, which is defined by the matrix elements

$$\tilde{V}_{kl} = \frac{1}{2}[\langle \tilde{\mathbf{u}}_k(\infty)\tilde{\mathbf{u}}_l(\infty) \rangle + \langle \tilde{\mathbf{u}}_l(\infty)\tilde{\mathbf{u}}_k(\infty) \rangle], \tag{S113}$$

for $k, l = 1, \dots, 8$. Under the stability condition, the covariance matrix $\tilde{\mathbf{V}}$ fulfills the Lyapunov equation

$$\tilde{\mathbf{A}}\tilde{\mathbf{V}} + \tilde{\mathbf{V}}\tilde{\mathbf{A}}^T = -\tilde{\mathbf{Q}}, \tag{S114}$$

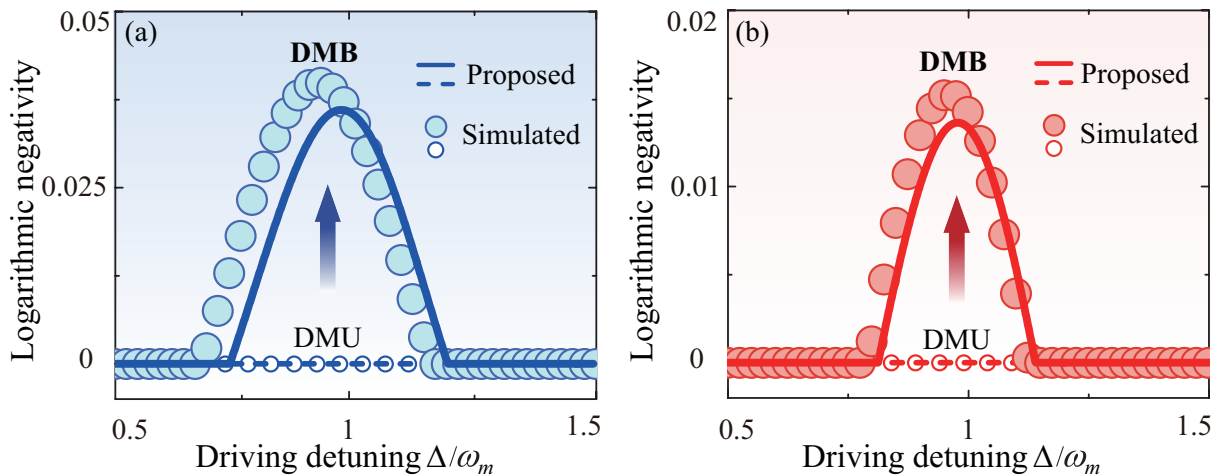


FIG. S13: Optomechanical entanglement measures $E_{N,j}$ versus the driving detuning Δ/ω_m in the DMU ($\chi = 0$, see the lower horizontal lines and symbols) and DMB ($V/\omega_j = 0.1$ and $\Theta = \pi/2$, see the upper curves and symbols) regimes. The curves show our proposed predictions, while the symbols correspond simulated results, which are obtained based on our suggested experimental system and parameters. Clearly, an excellent agreement between our proposed predictions and the simulated results is seen. This means that our proposed phenomena can be realized under current experimental conditions. Here we set $\Delta'_c = \Delta$ and $\Delta'_a/\omega_j = 5$, and other parameters used are shown in Table II.

where

$$\tilde{\mathbf{Q}} = \text{diag}\{\kappa_c, \kappa_c, \kappa_a, \kappa_a, \gamma_1(2\bar{n}_1 + 1), \gamma_1(2\bar{n}_1 + 1), \gamma_2(2\bar{n}_2 + 1), \gamma_2(2\bar{n}_2 + 1)\}, \quad (\text{S115})$$

which is defined by

$$\tilde{\mathbf{Q}} = (\tilde{\mathbf{C}} + \tilde{\mathbf{C}}^T)/2, \quad (\text{S116})$$

where $\tilde{\mathbf{C}}$ is the noise correlation matrix, defined by the matrix elements

$$\langle \tilde{\mathbf{N}}_k(s) \tilde{\mathbf{N}}_l(s') \rangle = \tilde{\mathbf{C}}_{k,l} \delta(s - s'). \quad (\text{S117})$$

Note that the optomechanical entanglement between the optical mode c and the j th mechanical mode d_j can be quantified using the logarithmic negativity $E_{N,j}$, as shown in Eq. (S34).

Notation	Remarks	Ref. [S10]	Our simulations
$\omega_j/2\pi$	Mechanical frequency of the j th resonator	6 GHz	6 GHz
$\kappa_{c(a)}/2\pi$	Optical decay rate of the c (a) cavity	1.03 (0.75) GHz	1.03 GHz
$g_{c(a)}/2\pi$	Single-photon coupling strength	0.76 (0.84) MHz	0.84 MHz
$n_{c(a)}$	Photon number in the c (a) cavity	10^3 (1.42×10^3)	5.1×10^5 (1.23×10^7)
n_j^h	Phonon number in the j th resonator	10	10
$\gamma_{1(2)}/2\pi$	Mechanical damping rate of the 1 st (2 nd) resonator	4.3 (5.9) MHz	1 MHz
$J/2\pi$	Photon-hopping coupling strength	$0.1 \sim 1$ GHz $< \omega_j$	4.8 GHz $< \omega_j$
$V/2\pi$	Phonon-hopping coupling strength	3 MHz $\ll \omega_j$	0.6 GHz $\ll \omega_j$

TABLE II: Parameters of the photonic-crystal optomechanical-cavity setup reported in the literature [S10] and used in our simulations. The columns 1 and 2 present the notation and physical meaning of the parameters used, respectively. The parameters in columns 3 and 4 are, respectively, used in the experimental works [S10] and our numerical simulations.

Next, we show in detail our numerical estimations to evaluate the experimental feasibility of the proposed scheme with the photonic-crystal optomechanical-cavity systems. To this end, we compare the relevance of the proposed results [based on Eq. (S1)] and the simulated results [based on Eq. (S106)] by performing numerical estimations. Here, the proposed results are determined by the three-mode optomechanical model proposed in the main text, while the simulated results are obtained based on the effective photonic-crystal optomechanical system, which is used to implement our three-mode target model by adiabatically eliminating one of the cavity modes. In Table II, we listed the experimental parameters used in the photonic-crystal optomechanical-cavity platform. For comparison, we also present the corresponding parameters of our numerical simulations, as shown in the right column of Table II. Note that this reported experiment focuses only on the realization of the nonreciprocity of

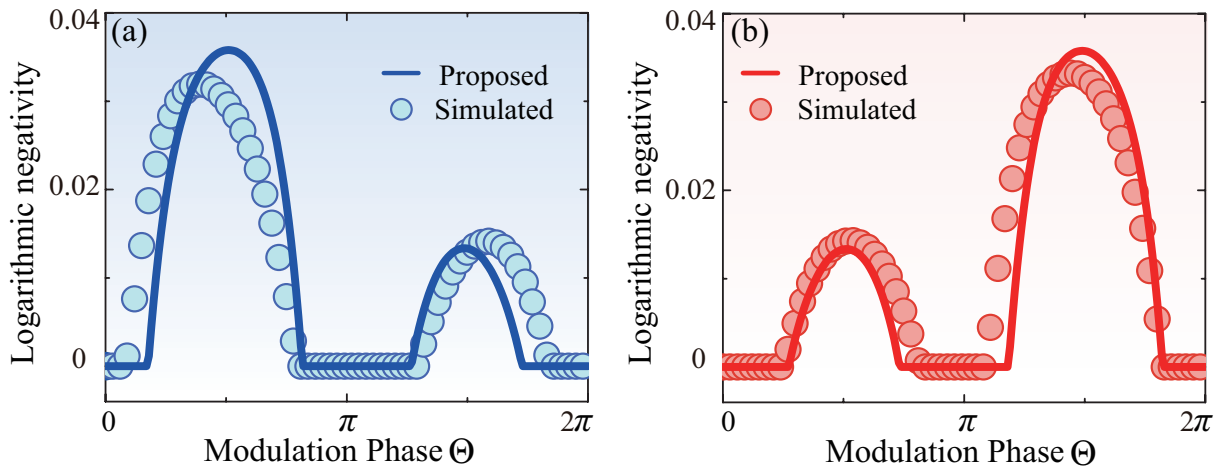


FIG. S14: Optomechanical entanglement measures $E_{N,j}$ as functions of the modulation phase Θ , where $\Delta'_c = \Delta = \omega_j$. The solid curves are our proposed predictions, while the symbols represent the simulated results. The excellent agreement between the proposed and simulated results indicates that the proposed phenomena are relevant for the state-of-the-art experiments. Here $\Delta'_a/\omega_j = 5$, and other parameters used are shown in Table II.

weak optical signals [S10], and therefore, it requires that the effective optomechanical couplings G_j , the photon-hopping coupling J , and phonon-hopping coupling V are much *smaller* than the mechanical resonance frequencies (i.e., small intracavity photon numbers $n_{c(a)} = 10^3$ (1.42×10^3), $J/2\pi \approx 0.1 \sim 1$ GHz $< \omega_j$, and $V/2\pi \approx 3$ MHz $\ll \omega_j$). However, to generate a *robust* dark-mode-immune and noise-tolerant entanglement, we need to *enhance* the optomechanical, photon-hopping, and phonon-hopping couplings. Therefore, we here have assumed the experimental achievable situations: $n_{c(a)} = 5.1 \times 10^5$ (1.23×10^7), $J/2\pi = 4.8$ GHz $< \omega_j$, and $V/2\pi = 0.6$ GHz $\ll \omega_j$. In addition, a single auxiliary cavity should be in the large-detuning regime $\Delta'_a \gg \omega_j$, such that this cavity-field mode can be adiabatically eliminated.

Based on both the proposed predictions and the simulated results, we display in Figs. S13(a) and S13(b) the optomechanical entanglement measures $E_{N,j}$ as functions of the driving detuning Δ of the cavity mode c , when the system operates in both the DMU and DMB regimes. Clearly, Figure S13 shows an excellent agreement between the proposed (curves) and simulated (symbols) results. Moreover, we find that in the numerical simulations based on both the proposed predictions and the simulated results, the optical mode and the mechanical modes are separable in the DMU regime ($E_{N,j} = 0$, see the lower horizontal lines and symbols), but they are entangled in the DMB regime [$E_{N,j} > 0$, see the upper curves and symbols]. These results indicate that our proposed phenomena are relevant for the state-of-the-art experiments.

To further show the dependence of the optomechanical entanglement on the synthetic magnetism, in Figs. S14(a) and S14(b), we plot the entanglement measures $E_{N,j}$ as functions of the modulation phase Θ by using both the proposed and simulated results. Here, the solid curves are plotted using the proposed results, while the symbols are based on the simulated results. We have shown that our proposed results and the simulated results are matched well with each other. In particular, we find that in the numerical simulations using both the proposed predictions and the simulated results, a multimode quantum device can be flexibly switched between separable and entangled states by tuning the modulation phase Θ . These numerical simulations imply that our physical model and the proposed phenomena can be effectively implemented under current experimental conditions in the photonic-crystal optomechanical-cavity systems.

B. Experimental realization of the proposed model based on the circuit electromechanical system

In this subsection, we propose another experimental implementation of the proposed physical model using the circuit electromechanical system [S2, S5, S26–S29], which consists of N micromechanical resonators (MRs) $d_{j=1\dots N}$ and a microwave cavity described by the equivalent inductance L and capacitance C , as shown in Fig. S15(a). Specifically, the displacement $x_{j=1\dots N}$ of each MR independently modulates the total capacitance through $C_{j=1\dots N}(x_j)$, and therefore the resonance frequency of the cavity ω_c . This leads to inducing the electromechanical coupling, which is described by $g_{j=1\dots N} = (\omega_c/2C)\partial C_j(x_j)/\partial x_j$. Meanwhile, an effective phase-dependent phonon-hopping interaction (i.e., the phase in a loop coupling induces an effective synthetic magnetism) between the nearest-neighbor MRs can be introduced by coupling them to a superconducting charge qubit, as shown in Fig. S15(b). The detailed derivation of an effective phase-dependent phonon-hopping coupling between the nearest-neighbor MRs is presented below.

In Fig. S15(b), a superconducting charge qubit is coupled to the two MRs. In this circuit, a Josephson junction (with

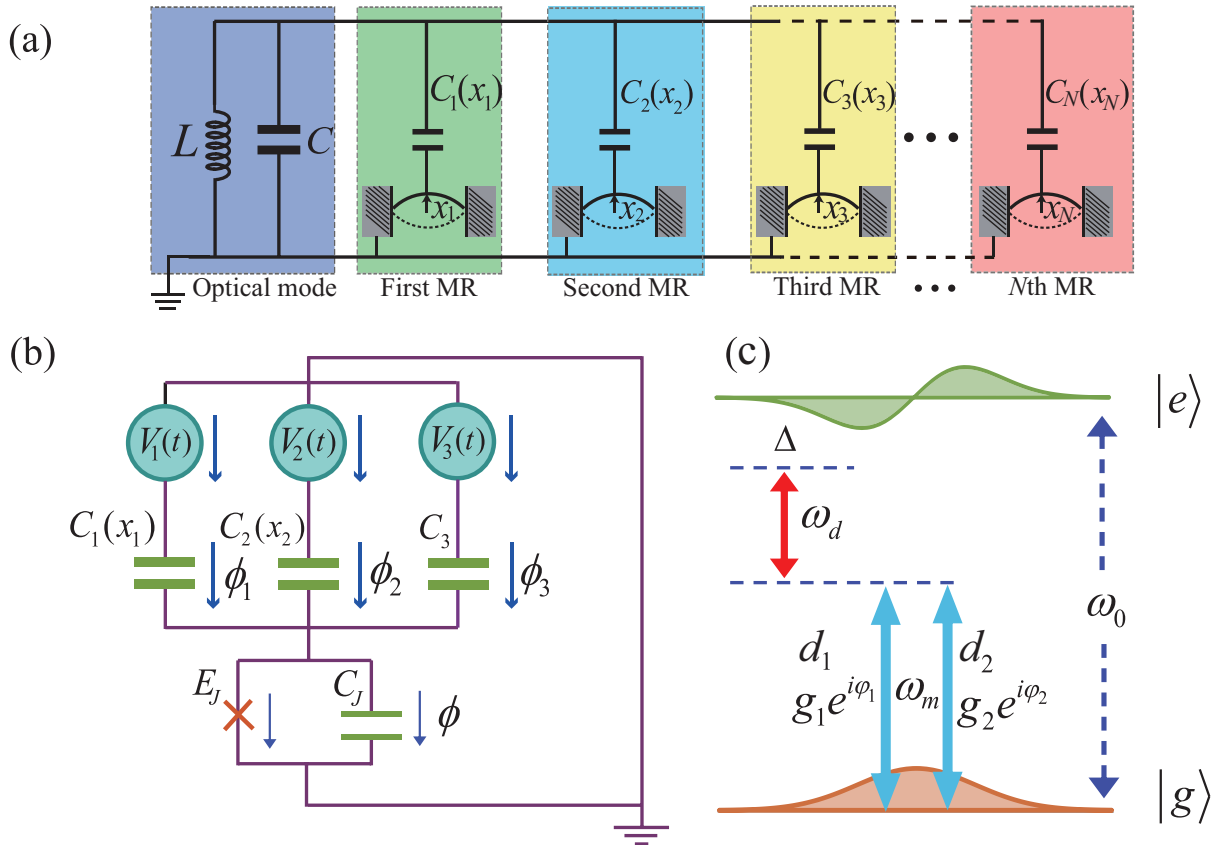


FIG. S15: (a) Schematics of a circuit electromechanical system consisting of a microwave cavity represented by $(N + 1)$ capacitances [C and $C_{j=1\dots N}(x_j)$] and an inductance (L). The j th capacitance $C_{j=1\dots N}(x_j)$ depends on the j th micromechanical resonator (MR) d_j . The displacement x_j of each MR modulates the total capacitance and hence the cavity frequency ω_c . The phase-dependent phonon-hopping interaction $\chi(e^{i\theta}d_1^\dagger d_2 + e^{-i\theta}d_2^\dagger d_1)$ between the nearest-neighboring MRs is generated via a superconducting circuit shown in panel (b). (b) Schematics of the superconducting quantum circuit: A Josephson junction with Josephson energy E_J and capacitance C_J is connected to three gate voltages $V_{j=1,2,3}(t)$ through the corresponding gate capacitances $C_{j=1,2}(x_j)$ and C_3 . Two MRs are coupled to the superconducting charge qubit through the gate capacitances $C_{j=1,2}(x_j)$. The gate voltages are properly designed such that a phase-dependent phonon-hopping interaction between the two MRs can be induced. The phase drops across these capacitors and the Josephson junction, and they are marked as ϕ_j and ϕ , respectively. (c) Energy levels and relevant resonance frequencies of this coupled qubit-resonator system. The two mechanical resonators with resonance frequency ω_m are phase-dependently coupled to the superconducting charge qubit with energy separation ω_0 . Through the gate capacitors, we apply ac gate voltages (with frequency ω_d) to the qubit.

capacitance C_J and Josephson energy E_J) is connected to three gate voltages $V_{j=1,2,3}(t)$ via the corresponding gate capacitances $C_{j=1,2}(x_j)$ and C_3 , in which the two gate capacitors with capacitances $C_{j=1,2}(x_j)$ are formed by one MR and one fixed plate, and the third capacitor has a constant capacitance. We denote the phase drops across these capacitors and the Josephson junction as ϕ_j and ϕ , respectively. In this circuit, the total kinetic energy, which is stored in these capacitors [S30], is written as

$$T = \frac{1}{2}C_J\dot{\Phi}^2 + \sum_{j=1,2} \frac{1}{2}C_j(x_j)\dot{\Phi}_j^2 + \frac{1}{2}C_3\dot{\Phi}_3^2, \quad (\text{S118})$$

where Φ and $\Phi_{j=1,2,3}$ denote the generalized magnetic fluxes, which are associated with the phase drops ϕ and ϕ_j across the Josephson junction and the capacitances C_j , respectively. We define the relation between the phase drop and the generalized magnetic flux as $\phi_{j=1,2,3} = 2\pi\Phi_j/\Phi_0$, with Φ_0 being the magnetic flux quanta. The Josephson energy is identified as the potential energy, which takes the form as $U = -E_J \cos\left(\frac{2\pi}{\Phi_0}\Phi\right)$ [S30], with E_J being the Josephson energy of this junction.

By using these voltages relations in these loops, the relations can be expressed as $V_j(t) + \dot{\Phi}_j + \dot{\Phi} = 0$, for $j = 1, 2, 3$, and then

we obtain the Lagrangian of this system:

$$L = T - U = \sum_{j=1,2} \frac{1}{2} C_j(x_j) V_j^2(t) + \frac{1}{2} C_3 V_3^2(t) + \frac{1}{2} \left(\sum_{j=1,2} C_j(x_j) + C_3 + C_J \right) \dot{\Phi}^2 + \left[\sum_{j=1,2} C_j(x_j) V_j(t) + C_3 V_3(t) \right] \dot{\Phi} + E_J \cos\left(\frac{2\pi}{\Phi_0} \Phi\right). \quad (\text{S119})$$

By introducing the momentum canonically conjugate to Φ , we obtain $P = \frac{\partial L}{\partial \dot{\Phi}} = \left[\sum_{j=1,2} C_j(x_j) V_j(t) + C_3 V_3(t) \right] + \left[\sum_{j=1,2} C_j(x_j) + C_3 + C_J \right] \dot{\Phi}$, and then the Hamiltonian of this circuit is derived as [S30]

$$H = \frac{1}{2} \frac{4e^2}{C_\Sigma(x_1, x_2)} \left[\hat{n} - n_g(x_1, x_2, t) \right]^2 - E_J \cos\left(\frac{2\pi}{\Phi_0} \Phi\right) - \frac{1}{2} \left[\sum_{j=1,2} C_j(x_j) V_j^2(t) + C_3 V_3^2(t) \right], \quad (\text{S120})$$

where the gate capacitance $C_\Sigma(x_1, x_2)$, the Cooper-pair number n , and the gate Cooper-pair number n_g are, respectively, defined by

$$C_\Sigma(x_1, x_2) = \sum_{j=1,2} C_j(x_j) + C_3 + C_J, \quad P = 2en, \quad \text{and} \quad n_g(x_1, x_2, t) = \frac{1}{2e} \left[\sum_{j=1,2} C_j(x_j) V_j(t) + C_3 V_3(t) \right]. \quad (\text{S121})$$

We below perform the quantization of this circuit by introducing the phase operator $\hat{\phi}$ and the number operator \hat{n} , and then, the Hamiltonian in the eigenrepresentation of the number operator can be expressed as

$$H = \frac{1}{2} \frac{4e^2}{C_\Sigma(x_1, x_2)} \sum_{n \in \mathbb{Z}} \left[n - n_g(x_1, x_2, t) \right]^2 |n\rangle \langle n| - \frac{E_J}{2} \sum_{n \in \mathbb{Z}} (|n\rangle \langle n+1| + |n+1\rangle \langle n|) - \frac{1}{2} \left[\sum_{j=1,2} C_j(x_j) V_j^2(t) + C_3 V_3^2(t) \right] \quad (\text{S122})$$

Here, we assume that this circuit works in the charge qubit regime $E_C \gg E_J$, with $E_C = 4e^2/C_\Sigma$ being the Coulomb energy. In addition, the gate charge in the vicinity of $1/2$ is chosen, such that the states $|0\rangle$ and $|1\rangle$ have almost degenerate energies. In this case, other states have higher energies, and thus, they can be safely ignored in our discussions. Then, the Hamiltonian in Eq. (S122) becomes

$$H \approx \frac{1}{2} \frac{4e^2}{C_\Sigma(x_1, x_2)} \left[n_g(x_1, x_2, t)^2 |0\rangle \langle 0| + [1 - n_g(x_1, x_2, t)]^2 |1\rangle \langle 1| \right] - \frac{E_J}{2} (|0\rangle \langle 1| + |1\rangle \langle 0|) - \frac{1}{2} \left[\sum_{j=1,2} C_j(x_j) V_j^2(t) + C_3 V_3^2(t) \right]. \quad (\text{S123})$$

We introduce the Pauli operators $\sigma_z = |0\rangle \langle 0| - |1\rangle \langle 1|$ and $|0\rangle \langle 0| + |1\rangle \langle 1| = I$, and the Hamiltonian in Eq. (S123) can be expressed as

$$H = \frac{1}{2} \frac{4e^2}{C_\Sigma(x_1, x_2)} \left[n_g(x_1, x_2, t) - \frac{1}{2} \right] \sigma_z - \frac{E_J}{2} \sigma_x + M, \quad (\text{S124})$$

where

$$M = \frac{1}{4} \frac{4e^2}{C_\Sigma(x_1, x_2)} \left[1 - 2n_g(x_1, x_2, t) + 2n_g^2(x_1, x_2, t) \right] - \frac{1}{2} \left[\sum_{j=1,2} C_j(x_j) V_j^2(t) + C_3 V_3^2(t) \right] \quad (\text{S125})$$

denotes the ac voltage driving term on the two MRs. We consider the case where the voltage drivings are far-off-resonance to the two mechanical vibrations, i.e., the driving frequencies of the two voltages are much smaller than the resonance frequencies of the two MRs. In this case, the term M can be safely discarded in our following discussions. Below, we assume that the distances between the fixed plate and the rest MR of the capacitors are much larger than the vibration amplitudes of the MRs, and thus, we can approximately express the capacitances as

$$C_j(x_{j=1,2}) \approx C_{j0} \left(1 - \frac{x_j}{l_j} \right), \quad (\text{S126})$$

where the parameters l_j and C_{j0} are, respectively, the rest distances between the fixed plate and the MRs in these gate capacitors and the capacitances of the gate capacitors when the MRs are rest. In addition, for our purpose we also choose the gate voltages: $V_{j=1,2}(t) = V_{j0} \cos(\omega_j t + \varphi_j)$ and $V_3(t) = (e - C_{10}V_1(t) - C_{20}V_2(t))/C_3$. In this case, we can easily obtain the following relation:

$$n_g(x_1, x_2, t) = \frac{1}{2} - \sum_{j=1,2} \frac{C_{j0}V_{j0}}{2e} \frac{x_j}{l_j} \cos(\omega_j t + \varphi_j). \quad (\text{S127})$$

We perform the rotation for the qubit $\sigma_z \rightarrow \tau_x$ and $-\sigma_x \rightarrow \tau_z$, and the Hamiltonian upto the first order of the mechanical displacements x_1 and x_2 can be obtained as

$$H_I \approx \frac{E_J}{2} \tau_z - \frac{E_C}{2} \left[\sum_{j=1,2} \frac{C_{j0}V_{j0}}{2e} \frac{x_j}{l_j} \cos(\omega_j t + \varphi_j) \right] \tau_x, \quad (\text{S128})$$

where $E_C = 4e^2/C_{\Sigma 0}$ under $C_{\Sigma}(x_1, x_2) \approx (C_{10} + C_{20} + C_J) \equiv C_{\Sigma 0}$. Note that the mechanical displacement terms in $C_{\Sigma}(x_1, x_2)$ only introduce the second-order terms of $x_{j=1,2}/l_j$, which have been neglected in our considerations. By including the free Hamiltonian of the two mechanical resonators and using the relations $x_{j=1,2} = \sqrt{\hbar/(2m\omega_m)}(d_j + d_j^\dagger)$ and $p_{j=1,2} = -i\sqrt{\hbar m\omega_m/2}(d_j - d_j^\dagger)$, the total Hamiltonian of this circuit system becomes

$$H_I \approx \omega_m \sum_{j=1,2} d_j^\dagger d_j + \frac{\omega_0}{2} \tau_z - \left[\sum_{j=1,2} g_j (d_j + d_j^\dagger) (e^{i(\omega_d t + \varphi_j)} + e^{-i(\omega_d t + \varphi_j)}) \right] (\tau_+ + \tau_-), \quad (\text{S129})$$

where we consider the case of $\omega_1 = \omega_2 = \omega_d$, and then we define the parameters: $g_j = \frac{E_C}{4} \frac{C_{j0}V_{j0}}{2e} \frac{x_{j0}}{l_j}$ and $\omega_0 = E_J$ with $x_{j0} = \sqrt{\hbar/(2m\omega_m)}$ being the zero-point fluctuation of the j th MR. To analyze the physical processes in this system, we now work in the rotating frame with respect to $H_0 = \omega_m \sum_{j=1,2} d_j^\dagger d_j + \frac{\omega_0}{2} \tau_z$, then we can obtain

$$\begin{aligned} V_I(t) = & -g_1(\tau_+ d_1^\dagger e^{i(\omega_0 + \omega_m + \omega_d)t} e^{i\varphi_1} + d_1 \tau_- e^{-i(\omega_0 + \omega_m + \omega_d)t} e^{-i\varphi_1}) - g_2(\tau_+ d_2^\dagger e^{i(\omega_0 + \omega_m + \omega_d)t} e^{i\varphi_2} + d_2 \tau_- e^{-i(\omega_0 + \omega_m + \omega_d)t} e^{-i\varphi_2}) \\ & -g_1(\tau_+ d_1^\dagger e^{i(\omega_0 + \omega_m - \omega_d)t} e^{-i\varphi_1} + d_1 \tau_- e^{-i(\omega_0 + \omega_m - \omega_d)t} e^{i\varphi_1}) - g_2(\tau_+ d_2^\dagger e^{i(\omega_0 + \omega_m - \omega_d)t} e^{-i\varphi_2} + d_2 \tau_- e^{-i(\omega_0 + \omega_m - \omega_d)t} e^{i\varphi_2}) \\ & -g_1(\tau_+ d_1 e^{i(\omega_0 - \omega_m + \omega_d)t} e^{i\varphi_1} + d_1^\dagger \tau_- e^{-i(\omega_0 - \omega_m + \omega_d)t} e^{-i\varphi_1}) - g_2(\tau_+ d_2 e^{i(\omega_0 - \omega_m + \omega_d)t} e^{i\varphi_2} + d_2^\dagger \tau_- e^{-i(\omega_0 - \omega_m + \omega_d)t} e^{-i\varphi_2}) \\ & -g_1(\tau_+ d_1 e^{i(\omega_0 - \omega_m - \omega_d)t} e^{-i\varphi_1} + d_1^\dagger \tau_- e^{-i(\omega_0 - \omega_m - \omega_d)t} e^{i\varphi_1}) - g_2(\tau_+ d_2 e^{i(\omega_0 - \omega_m - \omega_d)t} e^{-i\varphi_2} + d_2^\dagger \tau_- e^{-i(\omega_0 - \omega_m - \omega_d)t} e^{i\varphi_2}). \end{aligned} \quad (\text{S130})$$

This system has eight physical processes determined by the four detunings $\omega_0 + \omega_m \pm \omega_d$ and $\omega_0 - \omega_m \pm \omega_d$. From the viewpoint of the MRs and the qubit, the terms $\omega_0 - \omega_m \pm \omega_d$ and $\omega_0 + \omega_m \pm \omega_d$ are, respectively, the corotating terms and the counterrotating terms. Here, our aim of the introduction of the ac voltages $V_1(t)$ and $V_2(t)$ is that we can pick up the phase-sensitive interactions between the MRs and the charge qubit. To this end, the ac voltages with the frequency ω_d is chosen for picking up the terms with $\omega_0 - \omega_m - \omega_d$, i.e., the parameters satisfy the following conditions:

$$\omega_0 + \omega_m \pm \omega_d \gg \omega_0 - \omega_m + \omega_d \gg \omega_0 - \omega_m - \omega_d. \quad (\text{S131})$$

We find that the terms (with $\omega_0 + \omega_m \pm \omega_d$ and $\omega_0 - \omega_m + \omega_d$) are far-off resonant, and that the terms (with $\omega_0 - \omega_m - \omega_d$) are the target terms, which work in the large-detuning regime. The energy levels and these involved resonance frequencies of this coupled qubit-resonator system are shown in Fig. S15(c). In this case, the qubit-resonator interactions work in the large-detuning regime: $\Delta \gg g_{j=1,2} \sqrt{n_j}$, with n_j being the maximal excitation number in the j th vibration. Then, the phase-dependent photon-hopping interaction between the two MRs can be obtained, and this effective phase is the difference between the two phases φ_1 and φ_2 , which are associated with the qubit-resonator couplings. An approximate Hamiltonian, based on the above analyses, can be obtained as

$$V_I(t) \approx -\left[\tau_+ (g_1 d_1 e^{-i\varphi_1} + g_2 d_2 e^{-i\varphi_2}) e^{i\Delta t} + (g_1 d_1^\dagger e^{i\varphi_1} + g_2 d_2^\dagger e^{i\varphi_2}) \tau_- e^{-i\Delta t} \right], \quad (\text{S132})$$

where $\Delta = \omega_0 - \omega_m - \omega_d$. By going back to the Schrödinger representation, we can eliminate the time factor, and then write the Hamiltonian of the system as

$$H_{\text{eff}} = \omega_m \sum_{j=1,2} d_j^\dagger d_j + \frac{\omega_0 - \omega_d}{2} \tau_z - \tau_+ (g_1 d_1 e^{-i\varphi_1} + g_2 d_2 e^{-i\varphi_2}) - \tau_- (g_1 d_1^\dagger e^{i\varphi_1} + g_2 d_2^\dagger e^{i\varphi_2}). \quad (\text{S133})$$

In this work, we consider the case where the physical process associated with the detuning Δ works in the large detuning regime. As a result, the qubit coherence in the physical processes can be adiabatically eliminated, and then, we can obtain an effective

Notation	Remarks	Ref. [S26]	Our simutaions
$\omega_{1(2)}/2\pi$	Mechanical frequency of the 1 st (2 nd) resonator	10 (11.3) MHz	10 MHz
$\kappa/2\pi$	Cavity-field decay rate	1.38 MHz	2 MHz
$G_{1(2)}$	Effective optomechanical-coupling strength	0.1 ~ 0.5 MHz	2 MHz
$n_{1(2)}^{th}$	Phonon number in the 1 st (2 nd) resonator	41 (30)	100
$\gamma_{1(2)}/2\pi$	Mechanical damping rate of the 1 st (2 nd) resonator	106 (144) Hz	100 Hz
$\chi/2\pi$	Phonon-hopping coupling strength	no coupling	1 MHz \ll $\omega_{1(2)}$

TABLE III: Parameters of a circuit electromechanical system reported in the literature [S26] and used in our simulations. The columns 1 and 2 present the notation and physical meaning of the used parameters, respectively. The parameters in columns 3 and 4 are used in the experimental work [S26] and our numerical simulations, respectively.

phonon-hopping coupling between the two MRs by performing the second-order perturbation. By using the method of the Frohlich-Nakajima transformation [S31, S32], we can derive an effective Hamiltonian to describe the interactions. For this purpose, the effective Hamiltonian $H_{\text{eff}} = H_0 + H_I$ can be expressed as:

$$H_0 = \omega_m \sum_{j=1,2} d_j^\dagger d_j + \frac{\omega_0 - \omega_d}{2} \tau_z, \quad H_I = -\tau_+ (g_1 d_1 e^{-i\varphi_1} + g_2 d_2 e^{-i\varphi_2}) - \tau_- (g_1 d_1^\dagger e^{i\varphi_1} + g_2 d_2^\dagger e^{i\varphi_2}). \quad (\text{S134})$$

Furthermore, we introduce the operator $S = \frac{1}{\Delta} \tau_+ (g_1 d_1 e^{-i\varphi_1} + g_2 d_2 e^{-i\varphi_2}) - \frac{1}{\Delta} (g_1 d_1^\dagger e^{i\varphi_1} + g_2 d_2^\dagger e^{i\varphi_2}) \tau_-$, determined by the equation $H_I + [H_0, S] = 0$. This equation means that the first-order physical process is eliminated. An effective Hamiltonian describing the second-order physical interaction can then be obtained as

$$H'_{\text{eff}} = H_0 + \frac{1}{2} [H_I, S] = \sum_{j=1,2} \omega'_m d_j^\dagger d_j + \chi (d_1^\dagger d_2 e^{i\Theta} + d_2^\dagger d_1 e^{-i\Theta}) + \frac{\omega_0 - \omega_d}{2} \tau_z + \frac{(g_1^2 + g_2^2)}{\Delta} \tau_+ \tau_-, \quad (\text{S135})$$

where $\omega'_m = (\omega_m + \frac{g_j^2}{\Delta} \tau_z)$, $\chi = \frac{g_1 g_2}{\Delta} \tau_z$, and $\Theta = \varphi_1 - \varphi_2$. The above Hamiltonian shows that there is no transition in the qubit states, and that a conditional phase-dependent interaction between the two mechanical resonators is introduced. By assuming that the qubit is initial in its ground state $|g\rangle$ ($\tau_z |g\rangle = -|g\rangle$), we can obtain a phase-dependent phonon-hopping interaction (i.e., the phase in a loop coupling leads to a synthetic magnetism).

To demonstrate that the proposed phenomena are relevant for the state-of-the-art experiments based on the circuit electromechanical system (see Fig. S15), we present both the parameters reported in experiments and the parameters used in our numerical simulations, as shown in Table III. Note that all the simulations presented in the main text are based on these parameters (see Table III) related to the circuit electromechanical system. In these simulations, though we did not use the exact experimental parameters, all the used parameters are of the same order of magnitude of the reported parameters [S2, S5, S26, S27], and our used parameters are also often set in previous works [S1]. From the viewpoint of the experimental implementation, all the elements, except the phase-dependent phonon-hopping interaction, have been realized in experiments [S2, S5, S26, S27]. Therefore, a theoretical scheme for realizing the phase-dependent phonon-hopping interaction (i.e., the phase in a loop coupling leads to an effective synthetic magnetism) has been presented using the circuit electromechanical system in Sec. VB. These analyses indicate that the present scheme is experimentally accessible under current experimental conditions, and that the proposed phenomena can be observed in the state-of-the-art experiments based on the circuit electromechanical system.

-
- [S1] C. Genes, D. Vitali, and P. Tombesi, Simultaneous cooling and entanglement of mechanical modes of a micromirror in an optical cavity, *New J. Phys.* **10**, 095009 (2008).
- [S2] F. Massel, S. U. Cho, J.-M. Pirkkalainen, P. J. Hakonen, T. T. Heikkilä, and M. A. Sillanpää, Multimode circuit optomechanics near the quantum limit, *Nat. Commun.* **3**, 987 (2012).
- [S3] A. B. Shkarin, N. E. Flowers-Jacobs, S. W. Hoch, A. D. Kashkanova, C. Deutsch, J. Reichel, and J. G. E. Harris, Optically Mediated Hybridization between Two Mechanical Modes, *Phys. Rev. Lett.* **112**, 013602 (2014).
- [S4] M. C. Kuzyk and H. Wang, Controlling multimode optomechanical interactions via interference, *Phys. Rev. A* **96**, 023860 (2017).
- [S5] C. F. Ockeloen-Korppi, M. F. Gely, E. Damskäg, M. Jenkins, G. A. Steele, and M. A. Sillanpää, Sideband cooling of nearly degenerate micromechanical oscillators in a multimode optomechanical system, *Phys. Rev. A* **99**, 023826 (2019).
- [S6] C. Sommer and C. Genes, Partial Optomechanical Refrigeration via Multimode Cold-Damping Feedback, *Phys. Rev. Lett.* **123**, 203605 (2019).
- [S7] M. Schmidt, S. Kessler, V. Peano, O. Painter, and F. Marquardt, Optomechanical creation of magnetic fields for photons on a lattice, *Optica* **2**, 635 (2015).

- [S8] Z. Shen, Y.-L. Zhang, Y. Chen, C.-L. Zou, Y.-F. Xiao, X.-B. Zou, F.-W. Sun, G.-C. Guo, and C.-H. Dong, Experimental realization of optomechanically induced non-reciprocity, *Nat. Photonics* **10**, 657 (2016).
- [S9] F. Ruesink, M.-A. Miri, A. Alù, and E. Verhagen, Nonreciprocity and magnetic-free isolation based on optomechanical interactions, *Nat. Commun.* **7**, 13662 (2016).
- [S10] K. Fang, J. Luo, A. Metelmann, M. H. Matheny, F. Marquardt, A. A. Clerk, and O. Painter, Generalized non-reciprocity in an optomechanical circuit via synthetic magnetism and reservoir engineering, *Nat. Phys.* **13**, 465 (2017).
- [S11] N. R. Bernier L. D. Tóth, A. Koottandavida, M. A. Ioannou, D. Malz, A. Nunnenkamp, A. K. Feofanov, and T. J. Kippenberg, Nonreciprocal reconfigurable microwave optomechanical circuit, *Nat. Commun.* **8**, 604 (2017).
- [S12] Z. Shen, Y.-L. Zhang, Y. Chen, F.-W. Sun, X.-B. Zou, G.-C. Guo, C.-L. Zou, and C.-H. Dong, Reconfigurable optomechanical circulator and directional amplifier, *Nat. Commun.* **9**, 1797 (2018).
- [S13] F. Ruesink, J. P. Mathew, M.-A. Miri, A. Alù, and E. Verhagen, Optical circulation in a multimode optomechanical resonator, *Nat. Commun.* **9**, 1798 (2018).
- [S14] J. P. Mathew, J. d. Pino, and E. Verhagen, Synthetic gauge fields for phonon transport in a nano-optomechanical system, *Nat. Nanotechnol.* **15**, 198 (2020).
- [S15] Y. Chen, Y.-L. Zhang, Z. Shen, C.-L. Zou, G.-C. Guo, and C.-H. Dong, Synthetic Gauge Fields in a Single Optomechanical Resonator, *Phys. Rev. Lett.* **126**, 123603 (2021).
- [S16] E. X. DeJesus and C. Kaufman, Routh-Hurwitz criterion in the examination of eigenvalues of a system of nonlinear ordinary differential equations, *Phys. Rev. A* **35**, 5288 (1987).
- [S17] G. Vidal and R. F. Werner, Computable measure of entanglement, *Phys. Rev. A* **65**, 032314 (2002); M. B. Plenio, Logarithmic Negativity: A Full Entanglement Monotone That is not Convex, *Phys. Rev. Lett.* **95**, 090503 (2005).
- [S18] G. Adesso and F. Illuminati, Entanglement in continuous-variable systems: recent advances and current perspectives, *J. Phys. A* **40**, 7821 (2007); Continuous variable tangle, monogamy inequality, and entanglement sharing in Gaussian states of continuous variable systems, *New J. Phys.* **8**, 15 (2006); Entanglement sharing: from qubits to Gaussian states, *Int. J. Quantum Inf.*, **3** 383 (2006).
- [S19] J. Li, S.-Y. Zhu, and G. S. Agarwal, Magnon-Photon-Phonon Entanglement in Cavity Magnomechanics, *Phys. Rev. Lett.* **121**, 203601 (2018).
- [S20] V. Coffman, J. Kundu, and W. K. Wootters, Distributed entanglement, *Phys. Rev. A* **61**, 052306 (2000).
- [S21] R. Y. Teh and M. D. Reid, Criteria for genuine N -partite continuous-variable entanglement and Einstein-Podolsky-Rosen steering, *Phys. Rev. A* **90**, 062337 (2014).
- [S22] C. Genes, A. Mari, P. Tombesi, and D. Vitali, Robust entanglement of a micromechanical resonator with output optical fields, *Phys. Rev. A* **78**, 032316 (2008).
- [S23] H. Xu, D. Mason, L. Jiang, and J. G. E. Harris, Topological energy transfer in an optomechanical system with exceptional points, *Nature (London)* **537**, 80 (2016).
- [S24] H. Xu, L. Jiang, A. A. Clerk, and J. G. E. Harris, Nonreciprocal control and cooling of phonon modes in an optomechanical system, *Nature (London)* **568**, 65 (2019).
- [S25] M. Bhattacharya and P. Meystre, Multiple membrane cavity optomechanics, *Phys. Rev. A* **78**, 041801(R) (2008).
- [S26] C. F. Ockeloen-Korppi, E. Damskägg, J.-M. Pirkkalainen, M. Asjad, A. A. Clerk, F. Massel, M. J. Woolley, and M. A. Sillanpää, Stabilized entanglement of massive mechanical oscillators, *Nature (London)* **556**, 478 (2018).
- [S27] L. M. de Lépinay, C. F. Ockeloen-Korppi, M. J. Woolley, and M. A. Sillanpää, Quantum mechanics-free subsystem with mechanical oscillators, *Science* **372**, 625 (2021).
- [S28] Y.-x. Liu, J. Q. You, L. F. Wei, C. P. Sun, and F. Nori, Optical Selection Rules and Phase-Dependent Adiabatic State Control in a Superconducting Quantum Circuit, *Phys. Rev. Lett.* **95**, 087001 (2005).
- [S29] F. Massel, T. T. Heikkilä, J.-M. Pirkkalainen, S. U. Cho, H. Saloniemi, P. J. Hakonen, and M. A. Sillanpää, Microwave amplification with nanomechanical resonators, *Nature (London)* **480**, 351 (2011).
- [S30] M. Nakahara and T. Ohmi, *Quantum Computing: From Linear Algebra to Physical Realizations* (CRC Press, Boca Raton, 2008).
- [S31] H. Fröhlich, Theory of the Superconducting State. I. The Ground State at the Absolute Zero of Temperature, *Phys. Rev.* **79**, 845 (1950).
- [S32] S. Nakajima, Perturbation theory in statistical mechanics, *Adv. Phys.* **4**, 363 (1953).
- [S33] O. Gamel and D. F. V. James, Time-averaged quantum dynamics and the validity of the effective Hamiltonian model, *Phys. Rev. A* **82**, 052106 (2010).